UNSTEADY STATE MODELING OF LIQUID-LIQUID EXTRACTION PROCESSES WITH AXIAL DISPERSION

by

DON ALFRED BURGE

A DISSERTATION

Submitted in partial fulfillment of the requirements
for the degree of Doctor of Philosophy in the
Department of Chemical and Metallurgical
Engineering in the Graduate School
of the University of Alabama

UNIVERSITY, ALABAMA

1971

ACKNOWLEDGEMENTS

A personal note of gratitude is extended to the Cities Service Research and Development Company for fellowship support during my graduate study.

Dr. E. K. Landis first contacted me concerning the availability of the fellowship and was instrumental in processing my application for it, and for that I am indeed grateful.

I have been privileged in having Dr. W. C. Clements, Jr. as my research advisor. His counsel and influence are evident throughout my dissertation. I extend a sincere thanks to him and the other faculty members at the University of Alabama who have contributed to a rewarding experience.

ABSTRACT

The objective of this study was to develop and evaluate unsteady state models for liquid-liquid extraction with axial dispersion. A general model with axial dispersion in both phases was developed, and a methodology for evaluating the model's utility and estimating its parameters was discussed. A less general unsteady state model with axial dispersion only in the continuous phase was also developed, and its parameters were estimated by fitting Fourier transformed pulse test data to this dispersion model in the frequency domain. Data analysis using the dispersion model compares favorably with previously-published data with regard to estimated mass transfer coefficients and heights of a transfer unit. The derived model not only accounts for dispersion, but is a means for accurately estimating the dispersed phase holdup, and, indirectly, the specific interfacial area available for mass transfer (which is usually grouped with and considered a part of experimentally-determined mass transfer coefficients). Accurate estimates of dispersed phase holdup and its effect on overall coefficients and HTU's is a salient feature of the model presented, even for systems approaching plug flow. The estimated overall mass transfer coefficients based on the dispersed (organic) phase ranged from .018 to .0835 sec^{-1} and overall HTU's ranged from .13 to 1.07 ft. for a 3 inch diameter column, packed 5.63 ft. in length with 3/8 inch Raschig rings. The values of packed column Peclet numbers indicated that the system approached plug flow.

The model appeared to be more applicable (as indicated by better data fits) for large extraction factors, where dispersed phase mass transfer resistance is minimized. Averaged estimates of the individual heights of a transfer unit were .461 ft. for the continuous (aqueous) phase and .018 ft. for the discontinuous (organic) phase, in the range of large extraction factors where the best data fits to the dispersion model were obtained.

Parameters estimated from spray tower pulse tests (prior to packing the column) indicated excessive dispersion, low dispersed phase holdup, and small overall mass transfer coefficients when compared with packed tower operations at similar phase flow rates. The overall coefficients ranged from .00046 to .056 sec^{-1} and overall HTU's ranged from 3.7 to 26.2 ft. for representative spray tower pulse tests evaluated.

It was found that the dispersion model used in deriving the discontinuous (organic) phase transfer function predicts a time domain response whose shape is radically different from measured data curves, the extent of the difference depending on the degree of dispersion. Determining whether or not this predicted phenomenon is actually the case in a real-life situation would require a much faster measurement device than titration of averaged concentrations in organic samples taken intermittently during pulse testing.

TABLE OF CONTENTS

TABLE OF CONTENTS (continued)

LIST OF TABLES

LIST OF FIGURES

CHAPTER I

INTRODUCTION

Reported studies of distributed parameter models for liquid-liquid extraction, other than plug flow or single-phase dispersion models, have been extremely limited. In addition, there is a real need for definitive extraction models with both axial dispersion and mass transfer represented, particularly for extraction processes having automatic control, or other cases where a good correlation of the process dynamics is needed. This study was designed to advance the methodology of modeling such systems with as realistic a model as possible, within the limitations of the digital computer available.

The experimental portion of this study included pulse testing of both spray and packed columns. The length of the column used for mass transfer (i.e., the length from dispersed phase distributor at the column bottom to the interface level at the column top) was 171.5 cm (67.5 in.) and the cross-sectional diameter was 7.62 cm (3 in.). The packed column had the same dimensions and was packed with 3/8 inch Raschig rings. The fractional void volume of the packed column was 0.555.

The specific objectives of this study were: (1) to develop frequency domain extraction models for various assumptions concerned with mixing in each phase, (2) to determine the goodness of fit of the most realistic model within the confines of computer limitations, and (3) to estimate the parameters of the model chosen.

The model that was selected to be most representative of these requirements is based on an axial dispersion mechanism in the continuous phase and plug flow in the discontinuous phase. This is the model that was experimentally verified and subsequently used for parameter estimation. However, a theoretical basis for the more general case treating dispersion in both phases is also discussed.

Previously-reported extraction studies have used the assumptions of plug flow and steady state for determining experimental mass transfer coefficients. The problem with this approach is that the mass transfer coefficients so determined are not corrected for axial dispersion. Thus, if axial dispersion exists in a system, the calculated mass transfer coefficient would be smaller (due to the concentration gradient breakdown caused by axial dispersion) than for a plug flow system. As a result, if one attempts to extrapolate the experimental data of a short column to the design of a long column, the calculated number of transfer units would be significantly in error. The model proposed in this study is an attempt to overcome such scale-up problems.

CHAPTER II

LITERATURE REVIEW

Axial mixing is a common phenomenon in flow processes, but its significance in two-phase counter-current flow was not fully realized until researchers such as Geankoplis and Hixon (20) began reporting the effects of axial dispersion on extractor efficiency.

Brutvan (3), in an early report, determined axial dispersion coefficients of the continuous phase in a simulated spray tower using spherical glass beads to simulate the dispersed phase droplets. The localized Peclet numbers reported by Brutvan (3) and also by Hazelbeck and Geankoplis (24) on a methyl isobutyl ketone-water spray tower extractive system were based on the Danckwerts time domain solution (13) of the axial dispersion model for a step input using simplified boundary conditions. No attempt was made to determine dispersion coefficients and mass transfer coefficients simultaneously.

For steady state systems, mathematical relationships describing the axial mixing effect on extraction in counter-current systems were derived by Miyauchi and Vermeulen (34). They presented a generalized steady state mathematical treatment for the axial dispersion model in an extraction column, with a solution given for the exit raffinate concentration in terms of four independent parameters: (1) number of mass transfer units, (2) extraction factor, (3) continuous phase Peclet number, and (4) discontinuous phase Peclet number. In addition, simpler solutions for

special cases were offered where there are fewer degrees of freedom. For example, a solution was presented for the three-parameter steady state case where axial dispersion is absent in one phase.

Sleicher (46) attempted to relate the above four parameters to extraction efficiency. The generation of extraction efficiency values, if accurate, can then be the basis for more meaningful design calculations.

Clements (5), in the first of a series of related theses from Vanderbilt University, studied the dynamics of a packed column using pulse testing methods. Clements suggested that unsteady state data could be fit to a plug flow model, and the mass transfer coefficient could thus be determined. Although he was not able to actually analyze his data in this manner due to computer limitations, his work does represent the first attempt to use frequency domain results to determine model parameters for extraction. Clements also used a dispersion model for axial mixing without mass transfer in a determination of the dispersion characteristics in the aqueous phase of an extraction system. Later, Hays, Clements, and Harris (23) gave theoretical justification for the frequency domain evaluation of dynamic model equations, pointing out that Parseval's theorem is the key to a correct parameter evaluation algorithm. These matters are discussed further in Chapter VII.

Justice (26) and Elkins (17) continued the work of Clements, providing frequency response data from pulse tests of both spray and packed columns. Elkins first obtained estimates of Peclet number, based on the single phase dispersion model without mass transfer. Then, using an analog computer, with mass transfer coefficients varied slightly from the plug flow model, a comparison was made between the data and the equation for

time response. Good agreement was not obtained, and Elkins concluded that the analog used was not suitable for the analysis due to its limitations. None of the above investigations yielded satisfactory experimental and theoretical response comparisons when mass transfer was present.

Clements (6) presented a convincing argument, based on comparisons of the standard error of estimate for least squares fits of the dispersion model, for preferring the least squares estimation of parameters over that of the method of moments. He pointed out that the tail of a tracer response curve is weighted most heavily in the moments calculation, although it is the least precisely recorded portion of the curve. Also, the method of moments assumes prior knowledge that the model will fit. Clements used the Marquardt nonlinear least squares algorithm (31,32) for estimating parameters in the model, and presented the case for a frequency domain adaptation of the Marquardt algorithm when the time domain solution is not convenient or possible for the model being investigated.

Clements, in his thesis (5), also fitted his models in the Laplace domain, as did Williams and Adler in related work (52). The primary uncertainty in the Laplace domain modeling approach is the lack of theoretical basis for model error, as is available in the frequency domain through Parseval's theorem.

Jeffreson (25) discussed errors in frequency domain analysis and concluded, as did Clements (6), that moments analysis is less accurate than frequency domain least squares fitting. He also pointed out that tailing introduces error to both methods, and proposes a feedback control of the inlet variable upstream of the point of tracer injection to reduce tailing.

A study of procedures for Fourier transformation of the data was provided by Clements (5), Clements and Schnelle (7), and Pollock and Johnson (38). These studies help to assure accurate comparison of data to a frequency domain model through the use of efficient pulse testing and pulse reduction methods.

Sater and Levenspiel (41) used pulse testing to determine dispersion coefficients and holdup of two-phase flow in packed beds. Moment analysis was used to determine dispersion coefficients. No attempt was made to determine dispersion and mass transfer coefficients at the same time.

Brittan (2) reported a method for determining dispersion and mass transfer coefficients simultaneously, steady state axial concentration profiles being required as experimental data for parameter estimation. The disadvantage of his procedure lies in the difficulty of the experimental determination of reliable axial concentration profiles necessary for evaluation of accurate dispersion coefficients.

Considerable work has been done on a backmixing model that is essentially the same as a dispersion model except that it is a lumped parameter description of the mixing process rather than a distributed parameter description. This model was discussed by Miyauchi and Vermeulen (35), Li and Ziegler (30) and Mecklenburgh and Hartland (33). The model consists of perfectly mixed stages with specified stage height, each having the same volume. Exchange of material between two adjacent stages is due to bulk flows of main streams and to an additional back flow of the mixed phases, which occurs in each direction and is the sum of individual phase back flows. The back flow model can be shown to

be equivalent to the dispersion model when the total number of mixing cells approaches infinity.

An attempt by Doninger and Stevens (16) to simplify the dynamics of a packed column still further, using a lumped parameter model assuming perfect mixing cells in series, was unsuccessful. However, they were able empirically to determine correction factors for the magnitude ratio and phase angle.

Pollock and Johnson (39) examined the use of a variable mass transfer coefficient expressed as a function of concentration (or position) along the column. Concentration profile data and related mass transfer coefficients were reported. Good discussions of possible boundary conditions for dispersion models were given by Fan and Ahn (18), Levenspiel and Bischoff (28), Sheridan (43) and Wehner and Wilhelm (50).

An excellent historical review of reported axial dispersion studies in extraction columns and resultant conclusions were given by Pollock and Johnson (37).

Sherwood, Evans and Longcor (44) reported experimental mass transfer coefficients for a methyl isobutyl ketone-acetic acid-water system that are used for comparison in this study. Their experimental column was 3.5 inches in diameter and 54 inches in packed length, not too different from the 3 inch diameter, 67.5 inch packed length of the column used in the present study. Their volumetric rates were also in the same range. They used the well-known plug flow steady state derivation (47) for determining the mass transfer coefficients. Although, as previously discussed, the experimentally determined mass coefficients are usually too small if axial dispersion is present, there have been a

number of unusually large mass transfer rates reported for extraction systems, such as those reported by Garner and Hale (19), Karr and Scheibel (27) and Lewis (29). This phenomenon is commonly called the Marangoni effect, and is due to a spontaneous turbulent activity at the interface. This interfacial instability has increased mass transfer rates as much as tenfold or more over what would normally be expected.

CHAPTER III

THEORY

Restrictions and Assumptions of Models

The major restrictions of the models considered are: (1) The parameters (particularly Peclet number and mass transfer coefficient) do not vary with position or concentration along the column; (2) Drop dynamics of the organic phase are adequately described by the same mathematical considerations given to the continuous phase; (3) Radial turbulence is enough to assure uniform concentration radially (flat profile in the radial direction); (4) Mass is transferred according to the Whitman two-film theory (50); (5) Equilibrium exists at the interface; (6) The equilibrium relationship between the two phases is linear.

The plausibility of these assumptions is discussed at this point. The first assumption is not true, since it is known that the mass transfer coefficient is a function of concentration. However, the variation of this coefficient is not appreciable, particularly for the small range of concentrations used in the experimental portion of this study. The use of an effective column Peclet number is a common practice for convenience.

The second assumption can best be explained by Figure 1. Thus, the model is based on two continuous phases separated by a plane interface. One can deduce that if there is a uniform distribution of the dispersed phase droplets (no channeling) both radially and longitudinally in the

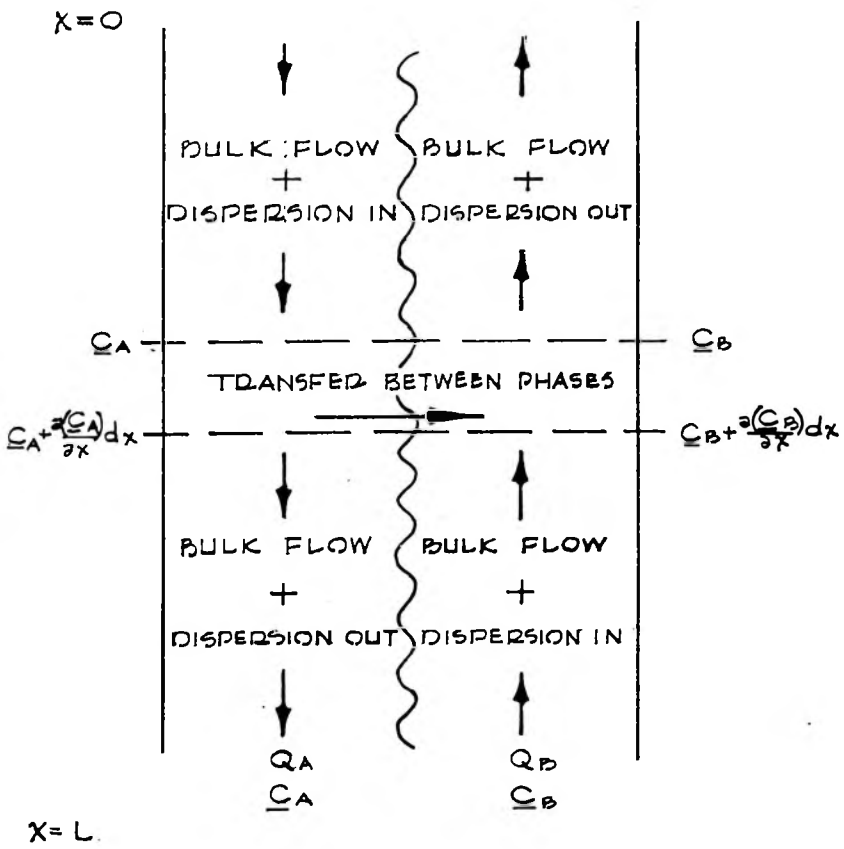

Figure 1. Transport Movement in Extraction Process

column, then the interfacial area associated with the droplets at a particular point in the column may be considered to be the same as that at any other point in the column, and a plane interface is a convenient analog representation. For the general model, where axial dispersion is assumed in both phases, it can only be said that a dispersive flow term superimposed on bulk flow to account for discontinuous phase longitudinal mixing is a convenient analog of the true mechanism whereby drops coalesce, collide, and are buffeted by the continuous phase in the axial direction. For lack of a better approach, it is a means of representing deviation from plug flow in the discontinuous phase. For the more restrictive of those models to be considered later, in which plug flow behavior in the discontinuous phase is assumed, the discontinuous dispersive term is zero, thus removing the approximation just described.

The third assumption, that of a flat concentration profile, is true for the highly turbulent flow patterns existing in most of the experimental runs made.

Assumptions 4 and 5 can be considered simultaneously, since assumption 5, equilibrium at the interface, is a part of the Whitman two-film theory, assumption 4. As Treybal (47) notes, the "two-film" theory should actually be called the "two-resistance" theory, since the film theory of mass transfer coefficients is not necessary or required. The Whitman theory merely contends that the only resistances to mass transfer are within the phases themselves. Thus, at the interface, the concentrations of both phases are at the equilibrium values, since there is no resistance to solute transfer across the interface separating the phases. There has been considerable evidence that assumption 5, that of equilibrium at the

interface, is true for ordinary situations, as Treybal also noted (47).

Assumption 6, that of a linear equilibrium relationship, is true for the methyl isobutyl ketone-acetic acid-water system over the concentration range used. A linear least squares fit of the data given by Scheibel and Karr (42) yields the following equilibrium relationship (see Appendix A) for $\underline{C}_A \leq .733$ g. mol./l. (The data for runs evaluated in this thesis is well below this maximum).

$$\underline{C}^*_B = -0.00663 + 0.525\underline{C}_A \tag{1}$$

Justice (26) has found that the distribution curve for this system is fairly insensitive to temperature variations over the temperature range used in this study. Hence, the distribution coefficient, m = .525, is used for models predicting deviations in concentration from steady state values, within the range for which the equilibrium data exhibits a linear characteristic.

Axial Dispersion in Both Phases, Model I

This model incorporates the most general of the various approaches discussed. It is based on a differential element cut along x, the direction of bulk flow. A mass balance is made on the solute in each phase, as illustrated in Figure 1.

For the aqueous phase, the following pertinent terms are listed:

Input Bulk Flow = $Q_A C'_A$

Input Dispersion Flow = $-D_A h_A (\partial C'_A / \partial x)$

Output Bulk Flow = $Q_A (C'_A + (\partial C'_A / \partial x) dx)$

$$\text{Output Dispersion Flow} = -D_A h_A(\partial C'_A/\partial x) - \frac{\partial}{\partial x}(D_A h_A \partial C'_A/\partial x)dx$$

$$\text{Output Mass Transfer to Organic Phase} = KaS\varepsilon(C'^{*}_{B} - C'_B)dx$$

$$\text{Accumulation} = h_A(\partial C'_A/\partial t)dx$$

Note that mass transfer from the aqueous phase to the organic phase is always assumed. The fractional void volume, ε, is 1.0 for spray tower operations and less than 1.0 for packed columns.

Next, using the conventional material balance relationship,

$$\text{Accumulation} = \text{Input} - \text{Output},$$

we arrive at the aqueous phase partial differential equation (note that deviations from steady state concentrations are used).

$$h_A(\partial C'_A/\partial t) = -Q_A(\partial C'_A/\partial x) - D_A h_A(\partial^2 C'_A/\partial x^2) - kS\varepsilon(mC'_A - C'_B) \quad (2)$$

Ka is replaced by k for convenience, since it is not convenient to separate the interfacial area per unit active volume of the column from the overall mass transfer coefficient. It should also be noted that the overall mass transfer coefficient is based on the dispersed phase, and thus C'^{*}_{B} is expressed in terms of C'_A in accordance with Equation 1.

A similar material balance on solute for the dispersed phase will yield

$$h_B(\partial C'_B/\partial t) = Q_B(\partial C'_B/\partial x) - h_B D_B(\partial^2 C'_B/\partial x^2) - kS\varepsilon(mC'_A - C'_B) \quad (3)$$

At this point, dimensionless length and concentration parameters are introduced:

$$Z = x/L \tag{4}$$

$$C_A = C'_A/C_{ref} \tag{5}$$

$$C_B = C'_B/C_{ref} \tag{6}$$

The substitution of Equations 4, 5 and 6 into Equations 2 and 3 yields the following two equations:

$$\theta_A(\partial C_A/\partial t) = -\partial C_A/\partial Z + (1/Pe_A)(\partial^2 C_A/\partial Z^2) - N_A(mC_A - C_B) \tag{7}$$

$$\theta_B(\partial C_B/\partial t) = \partial C_B/\partial Z + (1/Pe_B)(\partial^2 C_B/\partial Z^2) + N_B(mC_A - C_B) \tag{8}$$

where

$$\theta_A = h_A L/Q_A \tag{9}$$

$$\theta_B = h_B L/Q_B \tag{10}$$

$$N_A = kS\varepsilon L/Q_A \tag{11}$$

$$N_B = kS\varepsilon L/Q_B = N_A Q_A/Q_B \; ; \; H_{oB} = L/N_B \tag{12}$$

$$Pe_A = LQ_A/D_A h_A \tag{13}$$

$$Pe_B = LQ_B/D_B h_B \tag{14}$$

At this point, the two partial differential equations 7 and 8 are Laplace transformed with respect to time with initial conditions equal to zero, yielding two ordinary differential equations:

$$\theta_A s\bar{C}_A = -d\bar{C}_A/dZ + 1/Pe_A(d^2\bar{C}_A/dZ^2) - N_A(m\bar{C}_A - \bar{C}_B) \tag{15}$$

$$\theta_B s\bar{C}_B = d\bar{C}_B/dZ + (1/Pe_B)(d^2\bar{C}_B/dZ^2) + (N_A Q_A/Q_B)(m\bar{C}_A - \bar{C}_B) \tag{16}$$

where s is the independent variable of the Laplace transform with respect to time.

Equations 15 and 16 are now transformed with respect to the dimensionless distance variable Z:

$$\theta_A s\bar{\bar{C}}_A = -q\bar{C}_A + (1/Pe_A)q^2\bar{\bar{C}}_A - N_A(m\bar{\bar{C}}_A - \bar{\bar{C}}_B) \tag{17}$$

$$\theta_B s\bar{\bar{C}}_B = q\bar{C}_B + q^2\bar{\bar{C}}_B/Pe_B + N_A(m\bar{\bar{C}}_A - \bar{\bar{C}}_B) \tag{18}$$

where q is the independent variable of the Laplace transform with respect to Z.

Combining Equations 17 and 18 by eliminating $\bar{\bar{C}}_B$, one obtains the following fourth degree characteristic equation:

$$q^4/Pe_A Pe_B + q^3(1/Pe_A - 1/Pe_B) + q^2(-a_1/Pe_B - a_2/Pe_A - 1)$$
$$+ q(a_2 - a_1) + a_1 a_2 - N_A^2 Q_A m/Q_B = 0 \tag{19}$$

where

$$a_1 = \theta_A s + N_A m \tag{20}$$

$$a_2 = \theta_B s + N_A Q_A / Q_B \tag{21}$$

At this point, a solution of the fourth degree characteristic equation with complex coefficients would yield the Laplace domain solution,

$$\bar{C}_A(L,s) = P_1 e^{p_1} + P_2 e^{p_2} + P_3 e^{p_3} + P_4 e^{p_4}, \tag{22}$$

where p_1, p_2, p_3 and p_4 are the roots to the characteristic equation, and P_1, P_2, P_3 and P_4 are the coefficients. The coefficients can be determined by applying the following transformed boundary conditions:

$$\bar{C}_{in}(0^-,s) = \bar{C}_A(0^+,s) - (1/Pe_A)d\bar{C}_A(0^+,s)/dZ \tag{23}$$

$$d\bar{C}_A(1^+,s)/dZ = 0 \tag{24}$$

$$\bar{C}_B(1^-,s) + (1/Pe_B)d\bar{C}_B(1^-,s)/dZ = 0 \tag{25}$$

$$d\bar{C}_B(0^-,s)/dZ = 0 \tag{26}$$

These boundary conditions can be derived by performing material balances across the system's boundary planes, with the assumption that dispersion is negligible upstream of the inlet organic and aqueous feed streams and also negligible downstream of the aqueous and organic exit

points. The method of solution for and estimation of parameters for Model I in the frequency domain will become obvious after reading the next section treating Model II. The approach is the same for both models. Model I is not evaluated experimentally in this study, for reasons explained in the justification of Model II.

Axial Dispersion in Continuous Phase Only, Model II

The general model, previously developed, would be difficult to use in data fitting and estimation of parameters because of the large number of parameters, and also would be time consuming for computer calculations due to the necessity of solving a fourth degree characteristic equation with complex coefficients. Moreover, there is justification for simplification, since there is some evidence that the discontinuous phase Peclet number is considerably larger than the continuous phase Peclet number, as noted by Vermeulen et al. (49) and Burge (4). One is saved the difficult attempt to justify a dispersive coefficient for the discontinuous phase as was done previously, if it can be assumed that the discontinuous phase is in plug flow. This is the added restriction that distinguishes Model I from Model II.

One can perform a similar derivation, as was done for Model I, to arrive at two partial differential equations that can be manipulated to arrive at a third degree characteristic equation for Model II that is analogous to the fourth degree characteristic (Equation 19) for Model I. However, a simpler, faster approach is to let $Pe_B \to \infty$ in Equation 19. The resultant equation is

$$q^3/Pe_A + q^2(-a_2/Pe_A - 1) + q(a_2 - a_1) + a_1a_2 - N_A{}^2Q_Am/Q_B = 0 \quad (27)$$

Writing Equation 27 more concisely,

$$q^3 + dq^2 + eq + f = 0 \quad (28)$$

where

$$d = -(a_2 + Pe_A) \quad (29)$$

$$e = Pe_A(a_2 - a_1) \quad (30)$$

$$f = Pe_A(a_1a_2 - N_A{}^2Q_Am/Q_B) \quad (31)$$

Equation 27 has complex coefficients and complex roots. The solution of this characteristic equation is

$$\overline{C}_A(1,s) = B_1e^{m_1'} + B_2e^{m_2'} + B_3e^{m_3'}, \quad (32)$$

where roots m_1', m_2', and m_3' are functions of s.

The above Laplace domain equations can be transformed into the frequency domain by substituting jw for s. The frequency domain form is discussed later.

The appropriate boundary conditions include one boundary condition for the plug flow organic phase:

$$\overline{C}_B(1,s) = 0 \quad (33)$$

Model II boundary conditions for the aqueous phase are the same as those for Model I aqueous phase boundary conditions, since the continuous phase dispersion mechanism is the same for both models. These boundary conditions (Equations 23 and 24) are repeated here for clarity.

$$\bar{C}_{in}(0^-,s) = \bar{C}_A(0^+,s) - (1/Pe_A)d\bar{C}_A(0^+,s)/dZ \qquad (23)$$

$$d\bar{C}_A(1^+,s)/dZ = 0 \qquad (24)$$

The Laplace transformed equation that is descriptive of Model II aqueous phase solute behavior is the same as that for Model I (Equation 15) and is repeated here:

$$\theta_A s\bar{C}_A = -d\bar{C}_A/dZ + 1/Pe_A(d^2\bar{C}_A/dZ^2) - N_A(m\bar{C}_A - \bar{C}_B) \qquad (15)$$

The Laplace transformed equation that is descriptive of Model II organic phase solute behavior is the same as that for Equation 16, except there is no dispersive coefficient or Peclet number term since the organic phase is in plug flow. Thus the solute behavior for the plug flow organic phase for Model II is described by the transformed equation

$$\theta_B s\bar{C}_B = d\bar{C}_B/dZ + (N_A Q_A/Q_B)(m\bar{C}_A - \bar{C}_B) \qquad (34)$$

As mentioned previously, Equations 15 and 34 can be the basis for developing the aqueous phase characterisitic equation, Equation 27, or one can arrive at Equation 27 by taking the limit as $Pe_B \to \infty$ in Equation

19. These two equations are summarized at this point, since Equation 15 is the basis for determining the organic phase frequency domain solution.

The aqueous phase frequency domain solution is obtained from Equation 32 after substituting s = jw:

$$\overline{C}_A(1,jw) = A_1 e^{m}1 + A_2 e^{m}2 + A_3 e^{m}3, \tag{35}$$

where m_1, m_2 and m_3 are functions of w.

The organic phase frequency domain solution is obtained from Equation 15 after its transformation to the frequency domain. Letting s = jw:

$$\overline{C}_B(0,jw) = (N_A m + j\theta_A w)\overline{C}_A(0,jw) + d\overline{C}_A(0,jw)/dZ - (1/Pe_A)d^2\overline{C}_A(0,jw)/dZ^2 \tag{36}$$

where

$$d\overline{C}_A(0,jw)/dZ = A_1 m_1 + A_2 m_2 + A_3 m_3 \tag{37}$$

and

$$d^2\overline{C}_A(0,jw)/dZ^2 = A_1 m_1^2 + A_2 m_2^2 + A_3 m_3^2 \tag{38}$$

The roots m_1, m_2 and m_3 are found by a numerical technique described in a later section. After the boundary conditions (Equations 23, 24 and

33) are transformed into the frequency domain, substitutions of Equations 35, 37 and 38 into these boundary conditions yield three equations that are linear in the coefficients A_1, A_2 and A_3. These three equations are solved simultaneously to determine the coefficients. Since a scaling transformation was required to avoid excessive overflows and underflows in computations involving large Peclet numbers and mass transfer coefficients, the details of the computer solution for A_1, A_2 and A_3 will also be discussed in a later section.

Normalization of Transfer Functions Using Steady State Solutions

The characteristic equation, Equation 28, can be easily solved for the steady state form for the limiting case as $t \to \infty$ or $w \to 0$. When $w = 0$, the coefficient "f", defined in Equation 31, is zero. Therefore, Equation 39 is the steady state characteristic equation, where d_s and e_s are the same as d and e in Equations 30 and 31, evaluated at $w = 0$.

$$q^3 + d_s q^2 + e_s q = 0 \tag{39}$$

Obviously, one of the roots (m_{1s}) = zero, and the steady state aqueous phase output response is

$$\bar{C}_{As}(1,0) = A_{1s} + A_{2s} e^{m_{2s}} + A_{3s} e^{m_{3s}} \tag{40}$$

where

$$m_{2s,3s} = -(d_s/2) \pm \sqrt{(d_s^2 - 4e_s)}/2 \tag{41}$$

The organic phase output response is obtained from Equation 36 with w = 0:

$$\overline{C}_B(0,0) = N_A m\overline{C}_A(0,0) + d\overline{C}_A(0,0)/dZ - (1/Pe_A)d^2\overline{C}_A(0,0)/dZ^2 \qquad (42)$$

The procedure of normalization involved the solution for the coefficients of A_{1s}, A_{2s} and A_{3s} in terms of $\overline{C}_{in}(0,0)$ and the division of $\overline{C}_A(1,0)$ and $\overline{C}_B(0,0)$ by $\overline{C}_{in}(0,0)$ to obtain $G_A(1,0)$ and $G_B(0,0)$. There were also some scaling requirements for large values of the root m_{2s}, which will be discussed later. Finally, $G_A(1,jw)$ and $G_B(0,jw)$ were divided by $G_A(1,0)$ and $G_B(0,0)$, respectively, to obtain $G_{AN}(1,jw)$ and $G_{BN}(0,jw)$.

Determination of the Roots of the Aqueous Phase Characteristic Equation

As discussed previously, Equation 28, the aqueous phase characteristic equation, has complex coefficients and complex roots. One approach to finding the roots is suggested by Muller (36). In his technique, three arbitrary estimates, $m^{(0)}$, $m^{(1)}$ and $m^{(2)}$, of a desired root m_1 are first selected. The next estimate (an improvement over the three initial estimates) is determined by fitting a second degree Lagrangian interpolation equation to the points $[m^{(0)}, F(m^{(0)})]$, $[m^{(1)},F(m^{(1)})]$ and $[m^{(2)},F(m^{(2)})]$, and finding that next best estimate $m^{(3)}$ which is a root of the quadratic Lagrangian formula. The iteration is continued by dropping $m^{(0)}$ and repeating the quadratic fit for the points $m^{(1)}$, $m^{(2)}$ and $m^{(3)}$ to yield $m^{(4)}$. This iterative process is continued until

$|m^{(i)} - m^{(i-1)}|$ is as small as one desires. Once the root is found, the associated linear factor is divided into the polynomial, and, in the case of Equation 28 with three roots, the remaining two roots are found explicitly from the remaining quadratic expression.

The use of Muller's method for determining the roots of Equation 28 was attempted in this study. Initially, the algorithm appeared adequate, based on preliminary tests, for determining the roots. Later, however, it was found that packed column runs having high Peclet numbers and high organic holdup resulted in some large roots that produced convergence and inaccuracy problems. The basis for evaluating the accuracy of the root finding technique was calculation of the left side of Equation 28 with each of the estimated roots, to see how closely the magnitude approached zero. Although use of double precision arithmetic might have improved the method to an acceptable degree, it was decided to take an entirely different approach, as discussed below.

For the characteristic equation,

$$F(q) = q^3 + dq^2 + eq + f = 0, \tag{28}$$

where d, e and f are complex coefficients, another polynomial, F*(q), was formed, in which all the coefficients of F(q) were replaced by their conjugates. Then the two polynomials F(q) and F*(q) were multiplied together to form a sixth degree polynomial, $F_6(q)$, with only real coefficients. Since the new polynomial has real coefficients, Bairstow's method, discussed in detail by Ralston (40), could be used to find the roots. After the six roots of the new polynomial are found, the

computer algorithm picks the three roots out of the six that most nearly meet the requirement $|F(q)| = 0$. It was found that at least two estimated roots were excellent approximations to the actual roots of $F(q)$, but for some frequencies and parameter values the third estimated root was not much better than the other three roots of the sixth degree polynomial in approaching $|F(q)| = 0$. An additional refinement was added to the algorithm that resulted in three unique and extremely accurate roots. This refinement involves forming the third degree polynomial by multiplying the three linear factors $q - m_1$, $q - m_2$ and $q - m_3$ together. Thus, the unknown root m_3 is explicitly determined by equating like coefficients of $F(q)$ and the third degree polynomial $(q-m_1)\ (q-m_2)\ (q-m_3) = 0$, where m_1 and m_2 are given by Bairstow's method. It is believed that large magnitude differences in the real and imaginary parts of some of the coefficients of $F(q)$ were the cause for the needed refinement of Bairstow's method. The details of the computer algorithm will now be discussed.

The complex roots of a polynomial with real coefficients occur in conjugate pairs, each pair being the solution of a quadratic equation:

$$F_2(q) = q^2 + Hq + J = 0 \tag{43}$$

where H and J are real numbers. Thus, the process of finding the roots of the sixth degree polynomial

$$F_6(q) = C_1q^6 + C_2q^5 + C_3q^4 + C_4q^3 + C_5q^2 + C_6q + C_7 \tag{44}$$

can be regarded as equivalent to finding quadratic expressions which are factors of $F_6(q)$. Bairstow's method involves taking a trial quadratic expression, using trial values of H and J, to form Equation 43; dividing Equation 43 into Equation 44; and obtaining a fourth degree equation and the corresponding remainder. The fourth degree equation would be

$$F_4(q) = D_1q^4 + D_2q^3 + D_3q^2 + D_4q + D_5 \tag{45}$$

The remainder is of the form

$$R(q) = r_1q + r_2 \tag{46}$$

The algorithm is designed to choose successive values of H and J until r_1 and r_2 become zero. This is done by expanding r_1 and r_2 into a Taylor series and truncating after the linear term:

$$r_1(H + \Delta H, J + \Delta J) \simeq r_1(H,J) + (\partial r_1/\partial H)\Delta H + (\partial r_1/\partial J)\Delta J \tag{47}$$

$$r_2(H + \Delta H, J + \Delta J) \simeq r_2(H,J) + (\partial r_2/\partial H)\Delta H + (\partial r_2/\partial J)\Delta J \tag{48}$$

The partial derivatives can be found by first forming the sixth degree polynomial in the form

$$F_6(q) = F_2(q)F_4(q) + R(q) \tag{49}$$

where the right side of Equation 49 is obtained by combining Equations 43, 45 and 46 and the left side is Equation 44. By comparing like coefficients of the left side and right side of Equation 49, one can determine the partial derivatives of r_1 and r_2 in Equations 47 and 48. It is desired that r_1 and r_2 be zero. Therefore, Equations 47 and 48 are set equal to zero, and ΔH and ΔJ are solved for simultaneously to readjust H and J to successively better values until r_1 and r_2 are arbitrarily close to zero. Once the quadratic term is found, it is divided into the polynomial to reduce its degree, and the procedure is repeated until three quadratic factors and thus six complex roots are found.

As previously stated, a computer algorithm was developed for picking three roots out of the six that most nearly approach the requirement $|F(q)| = 0$. This was done by finding the absolute values of the deviation of $|F(q)|$ from zero, and picking the three smallest absolute values. Typical estimated values of $|F(q)|$ for at least two of the roots were of the order of 10^{-11} in magnitude. The third root, however, was not always significantly better than the other three roots of the sixth degree polynomial in approaching $|F(q)| = 0$. These remaining roots, when substituted in F(q), resulted in $|F(q)|$ being much greater than unity in most cases. It was decided to form the third degree polynomial

$$(q-m_1)(q-m_2)(q-m_3) = F(q) \tag{50}$$

where the complex roots

$$m_1 = m_{R1} + jm_{I1} \tag{51}$$

$$m_2 = m_{R2} + jm_{I2} \tag{52}$$

are found by Bairstow's method.

The remaining root defined as

$$m_3 = m_{R3} + jm_{I3} \tag{53}$$

is found by comparing like coefficients of Equations 28 and 50. For clarity, Equation 28 is repeated here.

$$F(q) = q^3 + dq^2 + eq + f \tag{28}$$

The real and imaginary parts of the root $m_3 = m_{R3} + jm_{I3}$ are

$$m_{R3} = - m_{R1} - m_{R2} - d_R \tag{54}$$

and

$$m_{I3} = - m_{I1} - m_{I2} - d_I, \tag{55}$$

where d_R and d_I are the real and imaginary parts of d, respectively. With this refinement, it was found that all three estimated roots of F(q) produced $|F(q)|$ values of the order of 10^{-11}. An examination of the Bairstow's method third root and the third root obtained from Equation

54 and 55 revealed that the imaginary part of the largest positive root was in error when computed by Bairstow's method, although the real part was correct. The large difference in the magnitudes of m_{R3} and m_{I3} apparently introduced inaccuracy in the Bairstow method computation.

Determination of Characteristic Equation Coefficients

Once the roots of the characteristic equation are determined, the next step in the computer algorithm for model frequency response computation is the determination of the coefficients of the characteristic equation in terms of $\overline{C}_{in}$. The boundary conditions, transformed into the frequency domain, are stated below.

$$\overline{C}_{in}(0,jw) = \overline{C}_A(0,jw) - (1/Pe_A)d\overline{C}_A(0,jw)/dZ \tag{56}$$

$$d\overline{C}_A(1,jw)/dZ = 0 \tag{57}$$

$$\overline{C}_B(1,jw) = 0 \tag{58}$$

By use of Equations 35 and 37 one can convert the three boundary conditions into linear equations expressing the coefficients A_1, A_2 and A_3. Thus the first boundary condition can be rewritten as

$$\overline{C}_{in}(0,jw) = A_1 + A_2 + A_3 - (m_1A_1 + m_2A_2 + m_3A_3)/Pe_A \tag{59}$$

Upon grouping terms,

$$A_1(1 - m_1/Pe_A) + A_2(1 - m_2/Pe_A) + A_3(1 - m_3/Pe_A) = \overline{C}_{in}(0,jw) \tag{60}$$

Equations 57 and 58 can be placed into a similar form,

$$A_1 m_1 e^{m_1} + A_2 m_2 e^{m_2} + A_3 m_3 e^{m_3} = 0 \tag{61}$$

$$A_1(a_1 + m_1 - m_1^2/Pe_A)e^{m_1} + A_2(a_1 + m_2 - m_2^2/Pe_A)e^{m_2} + A_3(a_1 + m_3 - m_3^2/Pe_A)e^{m_3} = 0 \tag{62}$$

Equation 62 is obtained by a direct application of Equation 36, with the organic response evaluated at $\overline{C}_B(1,jw)$.

It should be noted that the solution of the above coefficients at steady state (when $t \to \infty$) is the same as for the unsteady state, except they are evaluated as $w \to 0$.

Thus, the solution of the coefficients in terms of $\overline{C}_{in}(0,jw)$ from Equations 59, 60 and 61 is obvious. Once the coefficients are obtained in terms of $\overline{C}_{in}(0,jw)$, they are substituted into Equations 35 and 36. Then, with both sides of Equation 35 and 36 divided by $\overline{C}_{in}(0,jw)$, the transfer functions

$$G_A(1,jw) = \overline{C}_A(1,jw)/\overline{C}_{in}(0,jw) \tag{63}$$

$$G_B(0,jw) = \overline{C}_B(0,jw)/\overline{C}_{in}(0,jw) \tag{64}$$

are determined.

Similarly, the steady state solutions are

$$G_A(1,0) = \overline{C}_A(1,0)/\overline{C}_{in}(0,0) \tag{65}$$

$$G_B(0,0) = \overline{C}_B(0,0)/\overline{C}_{in}(0,0) \tag{66}$$

Then the normalized transfer functions are

$$G_{AN}(1,jw) = G_A(1,jw)/G_A(1,0) \tag{67}$$

$$G_{BN}(0,jw) = G_B(0,jw)/G_B(0,0) \tag{68}$$

Scaling Transformations for Boundary Condition Equations and Transfer Functions

Exponential overflows initially occurred in the computation which applied the Marquardt algorithm to the model. Diagnostic procedures revealed that the problem was due to a large positive root in the steady state solution, and a correspondingly large real part of a positive root in the transient solution of the model for some parameter estimates.

From Equation 41, in which d_s is a negative coefficient, one can see that the addition of the square root term in calculating m_{2s},

$$m_{2s} = -(d_s/2) + \sqrt{(d_s^2 - 4e_s)}/2, \tag{69}$$

results in m_{2s} always being positive and considerably larger than m_{3s}. The three boundary condition equations for the steady state that are analogous to the three boundary conditions (Equations 60, 61 and 62) for the transient state are

$$A_{1s} + A_{2s}(1 - m_{2s}/Pe_A) + A_{3s}(1 - m_{3s}/Pe_A) = \overline{C}_{in}(0,0) \tag{70}$$

$$A_{2s}m_{2s}e^{m_{2s}} + A_{3s}m_{3s}e^{m_{3s}} = 0 \tag{71}$$

$$A_{1s}N_A m + A_{2s}(N_A m + m_{2s} - m_{2s}^2/Pe_A)e^{m_{2s}} + A_{3s}(N_A m + m_{3s} - m_{3s}^2/Pe_A)e^{m_{3s}} = 0 \tag{72}$$

Note that m_{1s} is zero, as previously shown for the steady state solution.

From the previous discussion of Equation 69, the definition of m_{2s}, it can be assumed that exponential overflow problems would occur because of large values of m_{2s}.

If one examines Equations 71 and 72, it can be reasoned that the coefficient A_{2s}, associated with the large positive root m_{2s}, must be very small for this term to be of the same order of magnitude as the other terms with small roots. Hence a new coefficient was defined,

$$A'_{2s} = A_{2s}e^{m_{2s}} \tag{73}$$

Thus Equations 70, 71 and 72 can be rewritten as

$$A_{1s} + A'_{2s}(1 - m_{2s}/Pe_A)e^{-m_{2s}} + A_{3s}(1 - m_{3s}/Pe_A) = \overline{C}_{in}(0,0) \tag{74}$$

$$A'_{2s}m_{2s} + A_{3s}m_{3s}e^{m_{3s}} = 0 \tag{75}$$

$$A_{1s}N_A m + A'_{2s}(N_A m + m_{2s} - m_{2s}^2/Pe_A) + A_{3s}(N_A m + m_{3s} - m_{3s}^2/Pe_A)e^{m_{3s}} = 0 \tag{76}$$

From Equation 75, A'_{2s} is determined in terms of A_{3s}, and A_2's is consequently removed from Equations 74 and 76 by substitution. At this point it should be noted that the second term on the left-hand side of Equation 74 is very small if m_{2s} is large, because of the negative exponential containing the large positive number m_{2s}. Also, there is an exponential underflow if m_{2s} is too large. An arbitrary value of m_{2s} was picked (40 in the case of this study) as the maximum value at which the second term of Equation 74 is considered significant. For values of m_{2s} greater than this arbitrary number, the second term is set equal to zero. Diagnostic printouts during parameter estimation calculations confirmed the insignificance of the second term in Equation 74 for large values of m_{2s}. In any case, with A'_{2s} removed from Equations 74 and 76 by substitution of Equation 75, A_{1s} and A_{3s} can be determined in terms of $\overline{C}_{in}(0,0)$ and then, of course, A'_{2s} is subsequently determined. The steady state transfer functions are

$$G_A(1,0) = [A_{1s} + A'_{2s} + A_{3s}e^{m_3s}]/\overline{C}_{in}(0,0) \tag{77}$$

$$G_B(0,0) = [A_{1s}N_A m + A'_{2s}(N_A m + m_{2s} - m_{2s}^2/Pe_A)e^{-m_{2s}} + A_{3s}(N_A m + m_{3s} - m_{3s}^2/Pe_A)]/[N_A C_{in}(0,0)] \tag{78}$$

The second term on the right side of Equation 78 was found to be insignificant for large values of m_{2s} due to the exponential term, and was thus eliminated for values of m_{2s} greater than 40. The division by $\overline{C}_{in}(0,0)$ in Equations 77 and 78 simply cancels $\overline{C}_{in}(0,0)$, a linear factor in each of the numerator terms.

As one might suspect, the occurrence of exponential overflows in computations involving the steady state solutions were always followed by exponential overflows in the transient solutions. The source of the overflow was a large positive real part of one of the roots for some parameter values. The root finding technique, previously described, yields three roots not necessarily arranged in order of decreasing or increasing magnitude. Therefore, a computer algorithm was developed for ordering the three roots, with the largest positive real part designating the first root. This root is then A_1. A new coefficient A_1' was defined,

$$A_1' = A_1 e^{m_{R1}}, \tag{79}$$

where m_{R1} is the real part of m_1. Consequently, Equations 60, 61 and 62 can be rewritten as

$$A_1'(1 - m_1/Pe_A)e^{-m_{R1}} + A_2(1 - m_2/Pe_A) + A_3(1 - m_3/Pe_A) = \bar{C}_{in}(0,jw) \tag{80}$$

$$A_1' m_1 e^{jm_{I1}} + A_2 m_2 e^{m_2} + A_3 m_3 e^{m_3} = 0 \tag{81}$$

$$A_1'(a_1 + m_1 - m_1^2/Pe_A)e^{jm_{I1}} + A_2(a_1 + m_2 - m_2^2/Pe_A)e^{m_2} + A_3(a_1 + m_3 - m_3^2/Pe_A)e^{m_3} = 0 \tag{82}$$

Using the same logic for the transient boundary conditions (Equations 80, 81 and 82) that was applied to the steady state boundary

conditions (Equations 74, 75 and 76), the first term of Equation 80 was set equal to zero when m_{R1} was a large positive number to eliminate exponential underflows. Then A_1', A_2 and A_3 can be determined in terms of $\bar{C}_{in}(0,jw)$. The subsequent unsteady state transfer functions are:

$$G_A(1,jw) = [A_1' e^{jm}I1 + A_2 e^{m}2 + A_3 e^{m}3]/\bar{C}_{in}(0,jw) \tag{83}$$

$$G_B(0,jw) = [A_1'(a_1 + m_1 - m_1^2/Pe_A)e^{-m}R1 + A_2(a_1 + m_2 - m_2^2/Pe_A) + A_3(a_1 + m_3 - m_3^2/Pe_A)]/[N_A\bar{C}_{in}(0,jw)] \tag{84}$$

The first term of Equation 84 is set equal to zero when large positive values of m_{R1} are encountered, to prevent exponential underflows.

CHAPTER IV

EXPERIMENTAL APPARATUS

Description of System

The experimental system layout and flow diagram for the spray tower operation is shown in Figure 2. The packed column assembly and flow paths were the same as for the spray column, except, of course, the column was packed as described below.

The list of equipment used can be described under the four following headings: (1) Pyrex glass column, either empty or packed with 3/8 inch Raschig rings; (2) Feed stream polyethylene lines and storage tanks; (3) On-line continuous composition measurement for aqueous phase; (4) Off-line high precision micro-buret and attendant titration equipment.

Column and Packing

The column was constructed from sections of three-inch I.D. Pyrex glass pipe. The sections were connected by standard glass pipe couplings, with Teflon gaskets used for sealing purposes. The active column lengths, defined as the distance between distributor nozzles for the spray column and defined as the length of packed volume for the packed column, were equivalent for the spray and packed operations. This was achieved by maintaining the interface of the continuous aqueous phase just below the aqueous phase nozzle for both packed and spray columns, and with the interface located just above the column packing in the packed column runs.

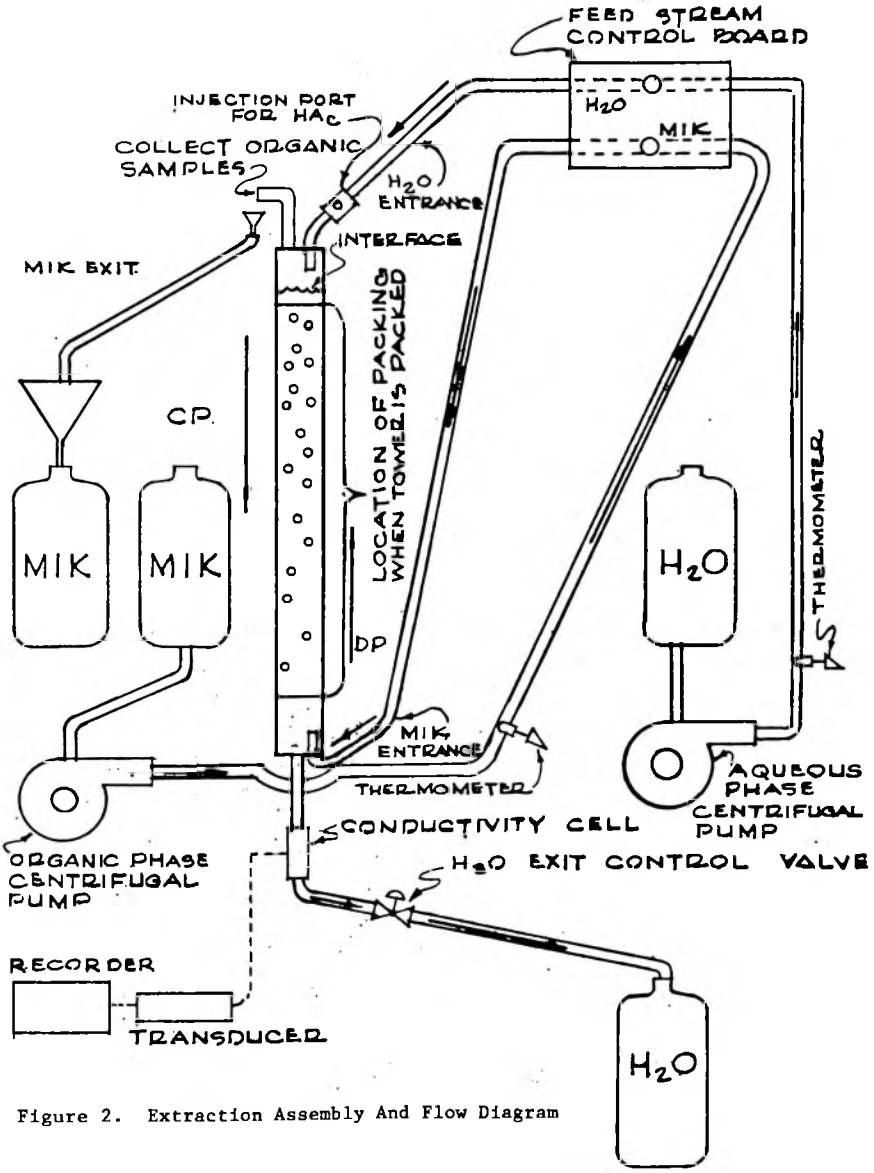

Figure 2. Extraction Assembly And Flow Diagram

(The location of the interface just above the packing improved the visual observation of interface movements, and thereby improved interface level control). The active length of the column as defined above was 171.5 cm (5 ft. 7.5 in.).

The packing support was a mesh having 5/16 inch openings and constructed from stainless steel. The packing used was 3/8 in. Raschig rings. Treybal (48) provides an empirical equation for calculating a minimum critical packing size:

$$d_{FC} = 2.42(\sigma/g\,\Delta\rho)^{0.5} \tag{85}$$

As noted from the variables, the critical packing size is a function of the raffinate-extract pair used, which is methyl isobutyl ketone-water for this investigation. The minimum calculated packing size for this pair is .205 in., safely below the 3/8 inch size used. Treybal (47) contends that packing sizes below this minimum result in drops of dispersed phase trapped by the interstices of the packing being unable to move forward except for random jostling by other drops and consequent coalescing and growth of the drops. Unusual and unpredictable hydrodynamic phenomena in systems involving small packings have been reported by Ballard and Piret (1).

The column was packed by dumping the Raschig rings into a liquid-filled tower to improve randomization and settling, as recommended by Treybal (48) and Gray (21). The column was operated several times, and liquid was drained each time to determine porosity until porosity appeared constant. When this had occurred, the column packing was

considered to be stable enough so that the system could be used further for dynamic testing. The void fractional volume of the packed column was $\varepsilon = .555$.

The nozzles used to distribute both aqueous and organic feed streams were 3/8 in. I.D. stainless steel tubes inserted vertically into the top and bottom of the column respectively.

Attendant Equipment

Centrifugal pumps (see Figure 2) were used for supplying both the dispersed organic phase (methyl isobutyl ketone) and the continuous phase (water) flow. Polyethylene piping provided the transport from feed tanks to the column and from the column to product tanks. Needle valves for flow control were located in the aqueous feed and exit lines and in the organic feed line. Thermometers for temperature measurement were located in aqueous and organic feed lines, and a tracer injection port was positioned just upstream of the column entrance in the aqueous feed line.

Aqueous Phase Composition Measurement

An electrical conductivity cell devised by Clements (8) was used in the aqueous exit line to monitor acetic acid concentration. The cell is made by inserting two platinum wires into a Teflon tube union, the wires being sealed at the point of entry by epoxy resin. The platinum surfaces exposed to the flowing stream were coated with platinum black, using a procedure recommended by Clements (9). The cell is first cleaned by filling with aqua regia. Next, the platinum wire ends are connected through wire leads to a source of about 3 volts direct current.

The direction of the current is reversed periodically over a 1-2 minute period. Then the cell is drained and rinsed thoroughly with distilled water. The cell is then immersed in a platinizing solution (3 grams of chloroplatinic acid and 0.02 grams of lead acetate per 100 cc. of distilled or deionized water) and the cell leads are connected again to a 3-volt direct current source. The direction of the current is reversed every 15 seconds until a uniform coating of platinum black is deposited on both electrodes. This process usually takes about three minutes. The electrodes are then rinsed in running water for about 45 minutes and stored overnight in distilled water, the water being drained and the cells refilled for two consecutive 24 hour periods before the cells are used. Thereafter, the cells are kept rinsed and filled with distilled water when the cells are not in use. Cells whose platinized surfaces become damaged or contaminated by deposits from the electrolytes in which they have been used should be recleaned with aqua regia, rinsed, and replatinized by the previously-described procedure.

The conductivity cell was inserted in the aqueous exit line just downstream of the column. The cell was connected through lead wires to a transducer that converts the conductivity measurement of the cell into a D.C. voltage of sufficient magnitude to accurately monitor with an electronic recorder. This transducer, also developed by Clements (8), was found to be accurate and reliable for sustained on-line monitoring. The complete circuit diagram for the transducer is given in Figure 3. A phase shift oscillator, operating at 1 kHZ, feeds a power amplifier. The amplifier is transformer-coupled to the measuring circuit, which consists of the conductivity cell and a series resistance Rs. The

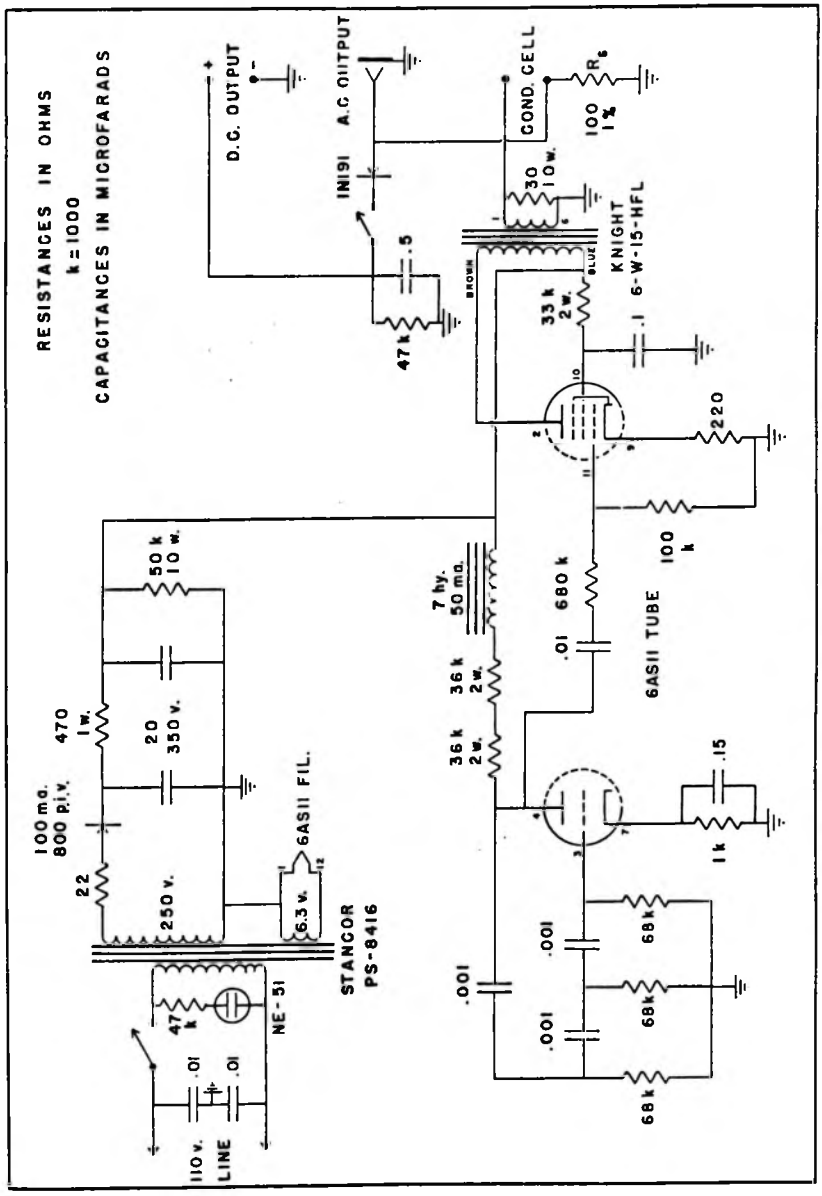

Figure 3. Schematic Diagram of The Electrical Conductivity Transducer

transducers were designed with R_s = 100 ohms by Clements, since the measured conductance L_c for most tracer work done in the University of Alabama Chemical and Metallurgical Engineering Department was expected to be less than 10^4 mhos. These values are based on Clements' recommendation that the highest value of L_c multiplied by R_s should approximate .01 for optimum linearity of calibration. However, some departure from linearity was observed at low tracer concentrations, since the small conductance values produced output voltages in the nonlinear range of the 1N191 diodes characteristic curve. Consequently, a polynomial fit of the data as described in the next section was performed to correlate accurately the conductance as a function of millivolt output. The output voltage of the transducer was recorded using a Honeywell Electronik-19 strip-chart recorder.

Organic Phase Composition Measurement

Organic extract samples containing dilute concentrations of acetic acid were collected at discrete time intervals during test periods. The samples were titrated with standard base, using a precision micro-buret with a 10 ml capacity and a platinum micro-tip for close control of standard solution drop size. Titrating procedure will be described later.

Calibration of Measurement Devices

There are three types of calibrations or correlations required for the aqueous phase composition measurement. These are: (1) Determination of the conductivity cell constant; (2) Determination of the best mathematical relationship between actual conductance (reciprocal of resistance) and the transducer output signal, and (3) Correlation of aqueous phase

acetic acid composition versus specific conductance with solution temperature as a parameter.

With the described relationships, the transducer output can be related to the conductance of the eletrolyte solution between the electrodes of the conductivity cell. The specific conductance then is determined by multiplying the cell constant by the cell conductance (or dividing by the cell resistance). Finally, the composition is found from a correlation of composition versus specific conductance with temperature as a parameter.

Conductivity Cell Calibration

The cell constant was determined by placing the flow cell in its line position downstream of the aqueous exit point and filling the extraction column as well as the cell with a standard solution of diluted acetic acid. The voltage from the transducer was recorded. Then a decade box connected to the transducer was used to determine the resistance (or reciprocal conductance, L_c) that corresponded to the recorded voltage. A portion of the standard solution drained from the cell was placed into a previously-standardized Leeds and Northrup conductivity cell to determine the specific conductance of the solution. From Daniels *et al.* (14) the specific conductance of the solution is:

$$L_s = K_{cs}/L_{cs} \tag{86}$$

where K_{cs} = cell constant for standard cell

L_{cs} = reciprocal resistance of standard cell

Then the unknown cell constant can be determined:

$$K_{cf} = L_s L_{cf} = L_s/R_{cf} \tag{87}$$

Several standard solutions with different acetic acid concentrations were used to obtain a good average value of the cell constant. This calibration process was repeated periodically during the months of cell usage. It was also done whenever there was reason to believe the cell constant may have changed, such as when the cell was replatinized. The calibration of the cell while located in its actual position in the system insured that the measured constant was not in error due to stray current paths present in the apparatus.

Transducer Calibration

Although the previously-described transducers are normally stable and reliable, failure of time-worn electrical components and recorder instability resulted in three different transducers and four different transducer calibrations being used. The transducers are labeled #5, #6 and #7. The #6 transducer was recalibrated after being turned on for an inordinately long time. Since this was done after the spray column tests and before the packed column tests, the calibrations are labeled accordingly. The #7 transducer was used for the last two packed column pulse tests. However, it was determined that the Honeywell recorder was the source of instability, and the recorder was also replaced. The calibrations were checked periodically to determine if calibration shifts occurred. Figure 4 is a calibration curve for the

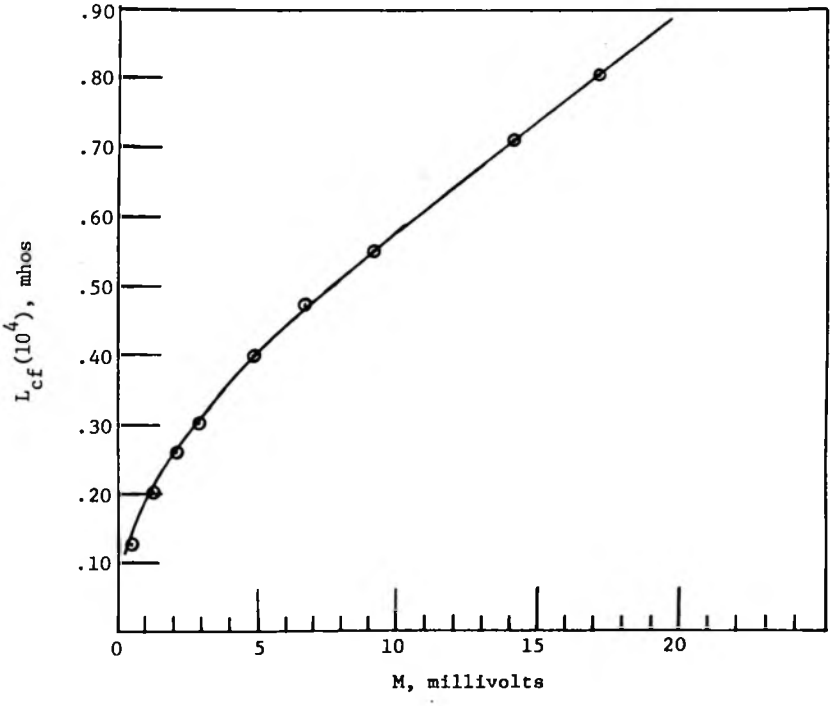

Figure 4. Calibration of No. 6 Transducer Used in Packed Column Operations

#6 transducer used for packed column tests, and is given as an example of the characteristic nonlinear relationship between cell conductance and transducer millivolt output for the low concentration range used. A series of polynomial least squares fits of cell conductance versus millivolt output signal from the conductivity transducer were made, with the fitted polynomials ranging in degree from 2 to 8. Consequently, it was decided that a fifth degree polynomial least squares fit reproduced very accurately the data for the range used in experimentation. The constants of the fitted equations are given in Appendix B. The transducers used for the specific tests are listed also in Appendix B.

Clements (5) gathered data for acetic acid composition versus solution specific conductance for a range of temperatures from 21°C to 33°C in two degree steps. He then developed a computer algorithm that computed composition from specific conductance. The algorithm also interpolated for solution temperatures that were in between those for which the experimental measurements were made. This computer algorithm was modified for use in this study. The previously-described correlations of conductance versus transducer millivolt output and the measured cell constant were used to generate specific conductance values that could then be converted to solution compositions by the computer algorithm. Hand calculations confirmed the validity of the computer algorithm.

CHAPTER V

DETAILS OF THE EXPERIMENTAL INVESTIGATION

Pulse Test Procedure

The pulse testing procedure was the same for both spray and packed columns. The following list of steps was employed during testing.

(1) A steady state flow rate was established for both continuous (aqueous) and discontinuous (organic) feed streams, with an interface level just below the continuous phase distributor and just above the column packing (for packed columns) at the top of the column. The approximate flow rate desired for a given test run was determined by valve position.

(2) Flow rates were calibrated using an electric timer and graduated cylinder.

(3) By monitoring the interface level and aqueous phase conductivity cell response, steady state interface level and concentrations could be determined. Sometimes, for low flow rates, or when interface level control difficulties were initially experienced, three to four hours were required to reach steady state. After steady state was reached, samples of aqueous and organic phase feed and exit streams were taken.

(4) After steady state samples were taken, 3 to 5 cubic centimeters of glacial acetic acid were injected rapidly with a hypodermic

needle into the aqueous feed line just upstream of the column.

(5) Immediately upon injection, the electric timer circuit was closed, and sampling of the extract was begun. The sampling intervals were 10 seconds initially; then increased to 15 seconds, 30 sec., 60 sec., 2 min., and 3 min., as the length of time since injection increased.

(6) During the sampling period, an eye was also kept on the conductivity transducer output recorder, and the time at which the leading edge of the acetic acid tracer cloud reached the conductivity cell was noted. This determined the dead time for the aqueous phase response.

(7) When steady state conditions were again achieved, as indicated by the conductivity transducer output returning to the original point, flow rates were again checked. Samples of the organic and aqueous phase exit streams were again taken.

(8) The three needle valves in the aqueous feed, aqueous exit, and organic feed streams were simultaneously closed.

(9) The column contents were dumped into a cylinder and the holdup of each phase was recorded.

Titration of Organic Phase Samples

The procedure for titrating organic phase samples was developed after considerable experimentation. An obvious problem was the low solubility of aqueous solutions in methyl isobutyl ketone. Acetone has been suggested as an additive to keep the solution being titrated as a single phase. However, it was found that methanol was superior to acetone, since less methanol was required, and the sharpness of the

end point was increased. The latter improvement may have been in part due to the fact that methanol was used to dissolve the phenolphthalein indicator.

It was found initially that a maximum of 6 ml of methanol added to a 10 ml pipetted sample of methyl isobutyl ketone-rich solution was required to keep the solution in a single phase for spray column operations. However, 8 ml of methanol was required for some of the samples taken during the packed column pulse tests, since the increased efficiency of the packed column increased the acetic acid concentration in some samples. Water-saturated solutions of acetic acid-free methyl isobutyl ketone were titrated to determine blank error (i.e., the excess amount of base required beyond the end point to visually see a color change). For the 6 ml methanol addition, the blank error was .19 ml, and for 8 ml, of methanol, the blank error was .33 ml. The corrected titrated volume is the volume of base less the volume of the blank, and was the volume used in calculating sample normalities.

Experimental Data

During packed column pulse tests, 25 dual sets of continuous phase and discontinuous phase (run numbers PW-1 to PW-25, run numbers PM-1 to PM-25) response data were collected. The aqueous phase data sets were converted to concentration units by the procedures discussed in Chapter IV. During spray tower operation, there were also 36 aqueous phase pulse tests (run numbers SW-1 to SW-36), 25 of these accompanied by discontinuous phase measurement response data collection (run numbers SM-12 to SM-36).

The aqueous and organic phase transfer function model equations expressing $G_{AN}(1,jw)$ and $G_{BN}(0,jw)$, previously described in Chapter III, were used to fit data from pulse tests of both packed and spray tower operations. Three parameters were estimated in the data fits, (1) overall mass transfer coefficient based on the organic phase, k; (2) fractional aqueous holdup, f_A; and (3) continuous (aqueous) phase Peclet number, Pe_A. The input data used to fit the model were unsteady state concentration-time data (C'_A or C'_B vs. t) and steady state volumetric rate data, Q_A and Q_B. The unsteady state concentration-time data were transformed into the frequency domain by the technique described in Chapter VI. The least squares fit in the frequency domain (see Chapter VI) yielded good estimates of the three parameters k, f_A and Pe_A, and hence, because of strong functional dependence upon these parameters allowed good estimates of θ_A, θ_B, h_A and h_B. The residence times θ_A and θ_B were previously defined in Equations 9 and 10, and h_A and h_B were calculated from f_A as follows:

$$h_A = f_A S\varepsilon \tag{134}$$

$$h_B = S\varepsilon - h_A \tag{135}$$

Also for completeness, the number of transfer units N_B and height of a transfer unit H_{oB} were calculated from Equation 12. Finally, representative model predictions were inverted back to the time domain for comparison with the time domain data.

It should be noted that six of the packed column pulse tests did

not yield good fits of the model, for reasons discussed in Chapter VIII. Five of the spray tower aqueous phase data sets were fitted to the model for comparison with the packed column operation.

CHAPTER VI

DATA TRANSFORMATION INTO THE FREQUENCY DOMAIN AND FOURIER INVERSION

The data collected in the experimental tests, after conversion to concentration units as previously described, must be transformed to the frequency domain to accomplish the least squares fits.

The Fourier transform is defined as

$$F(jw) = \int_0^\infty f(t)e^{-jwt}dt \tag{88}$$

and can be expanded using Euler's equation to obtain

$$F(jw) = \int_0^\infty f(t)\cos(wt)dt - j\int_0^\infty f(t)\sin(wt)dt \tag{89}$$

or

$$F(jw) = R(w) + j(I(w)) \tag{90}$$

where

$$R(w) = \int_0^\infty f(t)\cos(wt)dt \tag{91}$$

$$I(w) = \int_0^\infty f(t)\sin(wt)dt \tag{92}$$

Earlier investigators such as Clements and Schnelle (7) determined the Fourier transform directly using quadrature formulas. However, another more recent technique by Hays, Clements and Harris (23), that is demonstrably more efficient and flexible, has been used in this study, and is described below.

This technique approximates the f(t) curve by a series of polynomial segments. A discontinuity is allowed between segments. The time domain equation for the pulse test curve is equivalent to the summation of all the polynomial segments connected by a series of step functions. Parabolic segmentation was used in this study, although the technique was derived using polynomial segmentation of arbitrary degree.

For parabolic segmentation of the pulse curve, the summation of all parabolic segments is

$$f(t) \approx \sum_{i=1}^{n} \underline{u}(t - T_i)(\underline{A}_i + \underline{B}_i(t - T_i) + \underline{C}_i(t - T_i)^2) \tag{93}$$

The equation is then Laplace transformed to give

$$F(s) \approx \sum_{i=1}^{n} (\underline{A}_i/s + \underline{B}_i/s^2 + 2\underline{C}_i/s^3)e^{-T_i s} \tag{94}$$

Fourier transformation is achieved by substituting jw for s in Equation 94. This yields

$$F(jw) \approx \sum_{i=1}^{n} (\underline{A}_i/(jw) + \underline{B}_i/(-w^2) + 2\underline{C}_i/(-jw^3))e^{-jwT_i} \tag{95}$$

Using Euler's equation, substituting into Equation 95, and

collecting terms, the real and imaginary parts are

$$R(w) = \sum_{i=1}^{n} (\underline{A}_i/w + 2\underline{C}_i/w^3)\sin(wT_i) - \sum_{i=1}^{n} (\underline{B}_i/w^2)\cos(wT_i) \quad (96)$$

$$I(w) = \sum_{i=1}^{n} (-\underline{A}_i/w + 2\underline{C}_i/w^3)\cos(wT_i) + \sum_{i=1}^{n} (B_i/w^2)\sin(wT_i) \quad (97)$$

For a given value of w, the real and imaginary parts are calculated from Equations 96 and 97. A computer program was developed by Clements (10) to perform the previously-described Fourier transformation. The program was used in this study to determine the best frequency range for least squares fitting. Then, for this range of frequencies, the output of the algorithm supplied the input frequency domain data to the least squares program (12) as described in the next chapter.

The frequency domain least squares program by Clements (12) also provides for optional use of a Fourier inversion algorithm to generate tabulated and graphical comparisons of observed data to the model prediction.

The definition of the inverse Fourier transform for a real time function, f(t), is

$$f(t) = (1/\pi) \int_0^{\infty} F(jw)e^{jwt}dw, \quad (98)$$

where $f(t) = 0$ for $t < 0$.

It can be shown that f(t) can also be expressed in terms of the real part alone or the imaginary part alone (23). Thus,

$$f(t) = (2/\pi) \int_0^{\infty} R(w)\cos(tw)dw \tag{99}$$

$$f(t) = -(2/\pi) \int_0^{\infty} I(w)\sin(tw)dw \tag{100}$$

As pointed out by Hays, Clements and Harris (23) the integrals expressed in Equations 99 and 100 are exactly the same form as the integrals used for the direct Fourier transform expressed by Equations 91 and 92, except that t and w are interchanged. Of the two Equations, 99 and 100, Equation 100 is preferred for converting the frequency spectrum back to the time domain, since f(0) = 0 for data and models involved in this study (11,23). Therefore, using Equation 97, f(t) is computed as

$$f(t) \simeq -(2/\pi) \sum_{i=1}^{n} (-\underline{A}_i'/t - 2\underline{C}_i'/t^3)\cos(tW_i) + (2/\pi) \sum_{i=1}^{n} (\underline{B}_i'/t^2)\sin(tW_i). \tag{101}$$

CHAPTER VII

MODEL VERIFICATION AND PARAMETER ESTIMATION USING NONLINEAR LEAST SQUARES

Response Surface Search Techniques

These types of techniques are required when a model is nonlinear in its parameters, and when it is not desirable or possible to rearrange the model equation algebraically so that it becomes linear in all its parameters. Two recognized iterative methods for minimizing a function are: (1) Taylor series linearization, and (2) steepest descent. Marquardt (32) combined both into one algorithm, for reasons explained below.

The method of linearization involves expanding the model, $y_p = y(t,u,v)$ for example, into a Taylor series. For simplicity, the example model is chosen to have a single independent variable, t, and two parameters u and v.

If u_o and v_o are particular values of u and v, then a Taylor series expansion of y_p around u_o and v_o gives

$$y_p(t,u_o + \Delta u, v_o + \Delta v) = y_p(t,u_o,v_o) + \left.\frac{\partial y_p}{\partial u}\right|_{\substack{u = u_o \\ v = v_o}} \Delta u + \left.\frac{\partial y_p}{\partial v}\right|_{\substack{u = u_o \\ v = v_o}} \Delta v + (\text{terms of higher degree in } \Delta u \text{ and } \Delta v) \qquad (102)$$

The linearization of the above expansion is accomplished by truncation of the series beyond the linear terms.

For brevity, let

$$U_i = \left.\frac{\partial y_p}{\partial u}\right|_{\substack{u = u_o \\ v = v_o \\ t = t_i}} \tag{103}$$

and

$$V_i = \left.\frac{\partial y_p}{\partial v}\right|_{\substack{u = u_o \\ v = v_o \\ t = t_i}} \tag{104}$$

Also,

$$y_{poi} = y_p(t, u_o, v_o) \tag{105}$$

and

$$y_{pi} = y_{poi} + U_i \Delta u + V_i \Delta v \tag{106}$$

The usual method of least squares involve the minimization of the sum of the squares of the differences between the observed and predicted values of y by readjustment of the parameters. This procedure for a number, n, of discrete data points, is accomplished by minimizing ϕ, where

$$\phi = \sum_{i=1}^{n} (y_{oi} - y_{pi})^2 \tag{107}$$

or, for the model used as an example,

$$\phi = \sum_{i=1}^{n} (R_i - U_i \Delta u - V_i \Delta v)^2 \tag{108}$$

where

$$R_i = y_{oi} - y_{poi}. \tag{109}$$

The partial derivatives of ϕ with respect to Δu and Δv yield the two normal equations:

$$(\sum_{i=1}^{n} U_i^2)\Delta u - (\sum_{i=1}^{n} U_i V_i)\Delta v = \sum_{i=1}^{n} U_i R_i \tag{110}$$

$$(\sum_{i=1}^{n} U_i V_i)\Delta v - (\sum_{i=1}^{n} U_i^2)\Delta u = \sum_{i=1}^{n} U_i R_i \tag{111}$$

Solving for Δu and Δv simultaneously from Equations 110 and 111 gives the next approximation to the parameters,

$$u_1 = u_o + \Delta u \tag{112}$$

$$v_1 = v_o + \Delta v \tag{113}$$

Thus the linearization algorithm for two parameters is:

(1) First make initial guesses, u_o and v_o, for the parameters.

(2) From these guesses, the expressions for U_i and V_i are derived from differentiation of the equation being fit, or from numerical differentiation if analytical partial derivatives are difficult to obtain.

(3) Solve for Δu and Δv from the simultaneous Equations 110 and 111.

(4) Compute u_1 and v_1 from Equations 112 and 113.

(5) Substitute u_1 for u_o and v_1 for v_o, and repeat steps 1 and 2 until there is no further change in the parameters between successive trials.

There are refinements to the linearization method to improve convergence, such as halving the correction vector $(\Delta u, \Delta v)$ if $\phi_1 > \phi_o$ or doubling it if $\phi_1 < \phi_o$. Theoretically, as shown by Hartley (33), this method should always converge. However, in practice, nonlinearities in the model and poor parameter estimates can prevent convergence.

The steepest descent method involves concentrating on the sum of squares function, ϕ, and use of an iterative process to find the minimum of this function. For the example model, the basic idea is to move from an initial point (u_o, v_o) along the vector with components

$$- \partial\phi/\partial u \ , \ - \partial\phi/\partial v$$

whose values change continuously as the path is followed. One way of achieving this in practice, without evaluating functional derivatives, is to estimate the vector slope components at various places on the surface ϕ by fitting planar approximation functions, as detailed by Davies (15).

While the steepest descent method will theoretically converge, it may do so very slowly after some rapid initial progress. Slow convergence is particularly likely when the path of steepest descent zigzags slowly up a narrow ridge of the ϕ contour, each iteration bringing only a slight reduction in ϕ. Such contours are common in physical models.

The Marquardt algorithm uses steepest descent at the outset and linearization in the final stages, and thus attempts to utilize the best features of both methods; rapid minimization initially via steepest descent, and avoidance of slowdown due to ridges by use of the linearization methods.

Frequency Domain Nonlinear Least Squares

The Marquardt nonlinear least squares technique is useful when a time domain solution of a proposed model is practicable. It has also been adapted to the frequency domain as described by Hays, Clements and Harris (23). As noted by Clements (6), Parseval's theorem ensures that the results obtained in the frequency domain procedure are the same as would be obtained by a least squared analysis in the time domain.

The following discussion is based on notes and impressions gathered from a graduate course in mathematical modeling taught by Dr. Clements (11), and is an attempt to clarify the relationship between ϕ' in the time domain and ϕ' in the frequency domain.

For a continuous data response curve, ϕ' can be described by

$$\phi' = \int_{-\infty}^{\infty} (y_o(t) - y_p(t))^2 dt \qquad (114)$$

Note that negative time is allowed to make the discussion completely general. By substituting

$$e(t) = y_o(t) - y_p(t) \tag{115}$$

then

$$\phi' = \int_{-\infty}^{\infty} e^2(t)dt \tag{116}$$

Replacing one of the e(t) functions by its inverse Fourier transform, one obtains

$$\phi' = \int_{-\infty}^{\infty} \left[e(t)(1/2\pi) \int_{-\infty}^{\infty} E(jw)e^{jwt}dw \right] dt \tag{117}$$

The order of integration is reversed in the above double integral, giving

$$\phi' = 1/2\pi \int_{-\infty}^{\infty} E(jw) \left[\int_{-\infty}^{\infty} e(t)e^{jwt}dt \right] dw \tag{118}$$

The inner integral is the definition of E(-jw). Thus,

$$\phi' = 1/2\pi \int_{-\infty}^{\infty} E(jw)\ E(-jw)dw \tag{119}$$

If $E(jw) = R(w) + jI(w)$, (120)

then

$$E(-jw) = R(w) - jI(w). \tag{121}$$

Thus

$$E(jw)\ E(-jw) = \left(\sqrt{R^2(w)+I^2(w)} \right)^2 \tag{122}$$

or

$$|E(jw)|^2 = E(jw)\ E(-jw) \tag{123}$$

Then

$$\phi' = (1/2\pi) \int_{-\infty}^{\infty} |E(jw)|^2 dw \tag{124}$$

Since the above equation is obviously an even function of w,

$$\phi' = (1/\pi) \int_{0}^{\infty} |E(jw)|^2 dw \tag{125}$$

The definition of $|E(jw)|$ is

$$|E(jw)| = |Y_o(jw) - Y_p(jw)|. \tag{126}$$

Since $E(jw) = R_o(w) + jI_o(w) - R_p(w) - jI_p(w)$ (127)

Then

$$|E(jw)|^2 = (\Delta R)^2 + (\Delta I)^2, \tag{128}$$

where $\Delta R = R_o(w) - R_p(w)$ (129)

and

$$\Delta I = I_o(w) - I_p(w). \tag{130}$$

Thus the frequency domain expression for ϕ';

$$\phi' = (1/\pi) \int_o^\infty [(\Delta R)^2 + (\Delta I)^2] dw, \tag{131}$$

which is a special form of Parseval's theorem, allows the integral squared error function to be computed from frequency domain information.

In the computer algorithm by Clements (12), the observed values of $R_o(w)$ and $I_o(w)$, usually obtained from Fourier transformation of the pulse data, are used as input data to the least squares portion of the program. A user-supplied subroutine calculates $R_p(w)$ and $I_p(w)$ from the model equations being fitted. Then ϕ' is calculated by numerical integration, using the trapezoidal rule.

One has the alternative choices in frequency domain modeling of fitting data either to $G_p(jw)$ or to $Y_p(jw)$, whichever is desired. For fitting $Y_o(jw)$ data to $Y_p(jw)$, one can calculate $Y_p(jw)$ from

$$Y_p(jw) = G_p(jw)X(jw), \tag{132}$$

where $X(jw)$ is the transform of whatever forcing function was used to excite the dynamics of the process when it was tested. This is much easier than numerical convolution, which would be required for direct time domain calculation of $y_p(t)$.

Alternately, one could Fourier transform y(t) and x(t) data, and calculate the frequency response function

$$G_o(jw) = Y_o(jw)/X_o(jw). \tag{133}$$

Then one can fit the observed $G_o(jw)$ to the predicted $G_p(jw)$.

Since the normalized frequency content of a Dirac impulse function is unity, $G_o(jw) = Y_o(jw)$ for an impulse test. An impulse input can be closely approached in an experimental test upon a large capacity extraction column if the tracer pulse size is sufficiently large enough to allow accuracy in monitoring the output response, and if one can at the same time limit the pulse size to prevent nonlinearities such as a significant change in flow rates or in concentration-dependent parameters such as the distribution coefficient or the mass transfer coefficient. An impulse response was the experimental disturbance used in this study. Therefore, only the output response data for y(t) were required to determine $G_o(jw)$.

CHAPTER VIII

RESULTS AND CONCLUSIONS

Analysis of Characteristic Equation Roots

Exemplary sets of values of m_1, m_2, m_3, determined by the previously discussed root finding algorithm, and the resultant calculated value of F(q) for each of the determined roots over a range of frequency values are listed in Table 1. There are several points worth noting. For all of the sets of determined roots over the range of operating conditions of the system under study, one root always had negative real and imaginary parts and two roots always had positive real and imaginary parts. Also, one of the positive roots always had a predominately large real part. The magnitude of this positive real part became increasingly larger with increasing Peclet numbers, mass transfer coefficients and frequencies. As previously discussed, this large root, as a result of its increasing magnitude with changes in the parameters, introduced exponential overflows in computation of both the steady state and unsteady state roots. Diagnostic printouts indicated the steady state positive root and the unsteady state real part of the largest positive complex root were identical. Scaled boundary conditions and transfer functions, as previously discussed, brought calculations of the frequency domain model transfer function back within the range of computer capabilities. It is interesting to observe that the steady state set of roots (Chapter III) includes one

Table 1

Examples of Characteristic Equation Roots

w (Rad/Sec)	m_{Ri} (i= 1 to 3)	m_{Ii} (i= 1 to 3)	F(q) Real	F(q) Imaginary
.001	.818	.338	$-.333(10^{-14})$	0
	-.156	-.427	$.511(10^{-14})$	$.355(10^{-14})$
	101.01	.183	$-.217(10^{-10})$	$-.444(10^{-12})$
.01	-.780	-2.17	$.817(10^{-13})$	$.568(10^{-13})$
	1.409	1.275	$.675(10^{-13})$	$.170(10^{-12})$
	101.04	1.833	$.293(10^{-10})$	$-.108(10^{-11})$
.02	-1.01	-3.726	$-.284(10^{-12})$	$.114(10^{-12})$
	101.13	3.477	$.754(10^{-12})$	$-.122(10^{-8})$
	1.554	2.032	$.681(10^{-10})$	$-.322(10^{-10})$
.03	-1.22	-5.475	0	$.568(10^{-13})$
	101.28	5.291	$-.125(10^{-10})$	$-.169(10^{-9})$
	1.61	2.906	$.119(10^{-10})$	$-.978(10^{-11})$

positive, one negative, and one zero root. The root that is zero at steady state develops positive real and imaginary parts as w is increased from zero, because the coefficient, f, in the characteristic equation, Equation 28, possesses real and imaginary parts, and hence becomes significant in the characteristic equation solution. Finally, one can note in Table 1 that $|F(q)|$ is very close to zero for each of the estimated roots, a necessary requirement for judging the performance of the root-finding algorithm.

Packed Column--Aqueous Phase

Elkins (17) and Justice (26) have previously shown that pulses of acetic acid with volumes similar to this study can be injected into spray and packed column systems with even smaller capacities than the current investigation and still achieve linearity of dynamic response (constant flow rates, interface level, and other parameters). Therefore, it is concluded that the assumption of linearity is acceptable for the current study, lending support to the model's reliability in predicting the experimental system's dynamic response.

Nineteen data sets were fitted to the aqueous phase transfer function $G_{AN}(1,jw)$. For illustration, the reduced concentration data versus time after injection for four pulse tests are listed in Appendix C. The Fourier transformed data for the same four pulse tests, used as input data to the frequency domain least squares data fitting and parameter estimation program, are listed in Appendix D as examples of the Fourier transformation technique described in Chapter VI. Note that the largest frequency used is dependent on the maximum frequency associated with a normalized magnitude of $\approx .02$. This value was arrived at by Hays,

Clements, and Harris (23) as an optimum range for determining frequency content. For normalized magnitudes much lower than .02, there is a loss of significant digits in the calculation of frequency content, introducing error in the transformation calculations.

The estimated parameters k, f_A, Pe_A, integral squared error, ϕ'; flow rates Q_A and Q_B, and extraction factor mQ_B/Q_A are listed in Table 2 for the 19 fitted data sets. The estimated parameters N_B, H_{oB}, h_A, h_B, θ_A and θ_B are listed in Table 3. Values of ϕ' may be compared between runs here, rather than comparing standard errors of estimate or correlation coefficients, because the same number of samples of the frequency spectrum was used in all data fits.

An indication of the reproducibility of the data fits to the model is given in Table 4. Comparisons of the percent differences in estimated parameters, k and f_A, of duplicated pulse tests (similar operating conditions) are given. The duplicate pulse tests show an average of 7% difference in the value of k and 6% difference in the value of f_A. These differences are small considering that some flow rate and interface level variabilities are inherent, and any two pulse tests with truly duplicated operation conditions are not possible. The parameter Pe_A was not used for comparison since the packed column values of Pe_A are so large that the system approaches plug flow. Therefore, Pe_A does not significantly affect the response of the model. The worst data fits to the model were PW-5 and PW-17, and from Table 4, it is shown that these pulse tests had similar operating conditions. It can be noted that the fractional phase holdup (f_A) can be precisely estimated even for poor data fits, although k variability is large unless good data fits of the model are achieved. The significance of

Table 2

Packed Column Aqueous Phase Fitted Parameters and Operating Conditions

Test No.	k sec^{-1}	Pe_A	f_A	$\phi'(10^4)$	Q_A (cm^3/sec)	Q_B (cm^3/sec)	mQ_B/Q_A
PW-1	.0836	5833	.423	.4232	10.47	12.20	.612
PW-2	.0439	251903	.965	1.1230	5.30	19.0	1.88
PW-5	.0290	562	.985	2.4404	12.33	11.44	0.487
PW-7	.0642	7437	.302	.3342	5.05	6.55	.681
PW-8	.0277	2529	.365	.2796	4.97	10.55	1.115
PW-9	.0519	822	.501	.3724	9.94	15.15	.802
PW-10	.0447	20380	.611	.0374	9.94	15.50	.800
PW-11	.0703	2297	.636	.2879	14.08	16.90	.631
PW-12	.0767	1371	.510	.1409	14.00	18.45	.692
PW-13	.0376	14073	.778	2.1747	13.97	10.30	.388
PW-15	.0429	24278	.638	1.8659	13.90	13.21	.500
PW-16	.0455	139082	.563	.0154	9.87	10.85	.681
PW-17	.0172	58347	.990	4.4191	11.20	9.50	.445
PW-18	.0375	44867	.704	1.0358	10.65	7.83	.386
PW-19	.0195	1453	.990	4.6091	10.70	6.00	.295
PW-20	.0468	868	.502	.1156	7.63	12.80	.881
PW-21	.0486	22138	.443	.1363	8.12	9.90	.640
PW-23	.0186	71817	.906	.4437	7.82	15.40	1.032
PW-25	.0381	1856	.502	.4948	7.63	15.0	1.032

Table 3

Packed Column Aqueous Phase Fitted Parameters

Test No.	N_B	H_{oB} (ft.)	h_{A_2} (cm^2)	h_{B_2} (cm^2)	θ_A (sec)	θ_B (sec)
PW-1	29.70	.189	8.7	16.61	143	234
PW-2	10.01	.561	24.4	0.91	790	9
PW-5	11.00	.511	24.9	0.40	346	6
PW-7	42.50	.132	7.64	17.67	260	462
PW-8	11.35	.497	9.23	16.08	318	261
PW-9	14.85	.379	12.70	12.61	219	143
PW-10	12.80	.440	15.45	9.86	268	101
PW-11	18.00	.313	16.10	9.21	290	94
PW-12	18.70	.302	12.90	12.41	158	105
PW-13	15.80	.356	19.7	5.61	242	94
PW-15	14.10	.400	16.1	9.21	290	119
PW-16	18.20	.308	14.25	11.06	284	169
PW-17	7.80	.721	25.0	0.31	384	6
PW-18	20.60	.273	17.8	7.51	287	165
PW-19	14.10	.398	25.1	0.21	402	6
PW-20	15.4	.366	12.65	12.66	284	169
PW-21	21.4	.297	11.20	14.11	237	245
PW-23	5.25	1.075	23.0	2.31	503	26
PW-25	11.00	.511	12.70	12.61	286	144

Table 4

Percent Differences in Estimated Parameters
For Replicate Runs

Runs in Replicate Pairs	% Difference in k	% Difference in f_A
Comparison of Replicate Runs With Good Data Fits to The Model (Small Values of ϕ')		
PW-9 PW-10	7.45	9.1
PW-7 PW-19	6.00	0.0
PW-11 PW-12	4.55	9.4
Comparison of Replicate Runs With Poor Data Fits to The Model (Large Values of ϕ')		
PW-5 PW-17	25.6	.201
Comparison of Replicate Runs Where Interfacial Instability Was Possible ($Q_B/Q_A > 2$)		
PW-23 PW-25	34.2	28.6

large parameter estimate variability seen in duplicate runs PW-23 and PW-25 is discussed later in this section.

It is significant that large dispersed phase organic holdups h_B (or fractional dispersed phase holdup $1-f_A$) were characteristic of the seven data sets that were best fits to the model (lowest values of ϕ'). These seven "best fit" pulse tests were run numbers PW-8, PW-10, PW-11, PW-12, PW-16, PW-20, and PW-21. Large dispersed phase holdups could have been anticipated, since for all these "best fit" tests $Q_B/Q_A > 1$, with some values of Q_B/Q_A very much greater than 1.

Pulse tests PW-23 and PW-2, surprisingly enough, display low dispersed phase holdup, as estimated with the model, even though $Q_B/Q_A > 2$. The discrepancy may be due to the fact that there exists a potential for unstable and unpredictable phase holdups and interfacial area, possibly within incipient flooding, for volumetric ratios <0.5 or >2.0, as noted by Treybal (46). The degree of unpredictability in parameter estimates for $Q_B/Q_A > 2$ can be seen in Table 4 where duplicate pulse tests PW-23 and PW-25 are compared.

Sherwood, Evans, and Longcor (44) reported overall mass transfer coefficients based on the organic phase for the methyl isobutyl ketone-acetic acid-water system, their coefficients ranging from .0055 to .0244 sec^{-1} for a 5 ft. packed column with 3.5 inch diameter and packed with 1/2 inch rings. Flow rates used were comparable to those in the present study. Computed overall heights of a transfer unit, based on the organic phase, ranged from .59 to 1.56 ft. for the same data. The overall mass transfer coefficients in the current investigation ranged from .018 to .083 sec^{-1}, and the heights of a transfer unit

ranged from .13 to 1.07 ft. The agreement of this study with that of Sherwood et al. is very good, particularly in the light of mitigating circumstances. For example, the effects of the active aqueous and organic phase holdups (particularly unsteady state effects) and resultant residence times, estimated with the dispersion model, are not adequately accounted for in conventional steady state plug flow models as used by Sherwood et al . Also, it could be postulated that their 1/2 inch rings, being slightly larger than the 3/8 inch rings in this study, could have resulted in less dispersed phase holdup, reduced interfacial area, and increased dispersed phase resistance to mass transfer. The latter possibility is discussed in more detail later in this section.

Mass transfer coefficients, assuming a dilute solution (47), plug flow, and constant m, were calculated in the current investigation for seven data sets previously fitted to the dispersion model, and these values for mass transfer coefficient, number of transfer units and heights of a transfer unit are listed in Table 5. It can be noted that these coefficients are much smaller than the coefficients estimated from the dispersion model. The very small steady state concentrations used to assure dilute solutions and constant m resulted in very small concentration differences to be measured by titration. This would suggest that the mass transfer coefficient calculation for the steady state may be inaccurate due to the increased significance of experimental error in computing differences of small concentrations.

There is also the possibility that the assumption of a constant mass transfer coefficient, one independent of concentration, is not a valid assumption when comparing the low concentration steady state mass transfer

Table 5

Transfer Coefficients and Related Parameters
Based on Steady State Plug Flow Equation

Test No.	k (sec^{-1})	N_B	H_{oB} (ft.)
P-8	.000767	.315	17.9
P-10	.000403	.115	48.7
P-11	.001140	.293	19.2
P-16	.000665	.265	21.2
P-20	.000671	.227	24.4
P-21	.000605	.265	21.2
P-23	.000472	.132	42.5

coefficient with the mass transfer coefficient obtained from runs at higher concentration levels. A phenomenon that could also be a factor is interfacial turbulence, known as the Marangoni effect (19), during unsteady state pulsing of the concentration. The Marangoni effect, as previously discussed, can cause unusually large mass transfer rates. However, this possibility is discounted if it can be assumed that the comparable steady state data of Sherwood et al. was not obtained under the influence of the Marangoni effect.

Large Peclet numbers for packed column operation were also expected. The very high Peclet numbers obtained may have been due to the length of the column and the large L/S ratio, reducing the significance of end effects and column diameter that contribute to the degree of dispersion. Short packed columns with large diameters have higher degrees of dispersion, as verified by comparing reported dispersion coefficients of Hazelbeck and Geankoplis (23), obtained from a short column with a large diameter, with the coefficients reported by Elkins (17), obtained from a longer column and shorter diameter.

The significance of the effect of organic holdup on the mass transfer coefficient is seen in the data of Table 3, where mass transfer coefficients are obviously larger when organic holdups h_B are large. The ability to estimate good values for the "active" organic and aqueous phase holdups and to determine their effects on mass transfer is one of the salient features of the dispersion model presented. The term "active" holdup is used to differentiate it from the commonly-mentioned term, normal holdup, that is obtained by stopping the flow of liquids to the column, allowing the dispersed phase to settle, and measuring the

drained volumes. By contrast, the active holdup is the actual holdup available for mass transfer, and is a function of the degree of dispersion and other factors such as the packing size, drop size and the potential affinity of one of the phases for the packing material. Also, the amount and composition of the material that does not drain from the column (a factor in active holdup) has an unknown significance on subsequent extraction runs. Estimation of phase holdups using the dispersion model developed in this study could be important in determining the active phase holdups and studying their effect on the system's variables affecting column performance. Large organic holdups for the packed column operations provided long enough residence times in the organic phase for effective mass transfer to occur.

The importance of maintaining as high an organic holdup as possible can be easily shown by an equation defining the interfacial area per unit volume for a packed column,

$$a = 6\varepsilon(1-f_A)/d_p \tag{136}$$

The above equation can be derived by taking the ratio of the surface (πd_p^2) and volume ($\pi d_p^3/6$) of a dispersed phase drop, assuming the drop is spherical, with corrections for the fractional dispersed phase holdup and void volume of the column. Thus, it is evident that maintaining as large as possible a value for the fractional organic phase holdup, $(1-f_A)$, within the limitations of stability, is most essential in optimizing extraction processes. Conventional methods of obtaining $(1-f_A)$ by dumping and measuring the column contents do not adequately

measure the active holdup as described previously. Design techniques based on a correlation by Zenz (53) have been given for estimating the slip velocity and resultant relationship between Q_A, Q_B and $(1-f_A)$, but these computations are very approximate. It is believed that the dispersion model, developed and evaluated in this study, would be most useful in giving the designer more realistic computations of $(1-f_A)$ and specific interfacial area than have been previously available, even for systems approaching plug flow.

The dispersion model with the estimated parameters was inverted to predict C'_A in the time domain and compare it with the observed data. These comparisons in tabular form for four evaluated test runs that were especially good fits to the model are given in Appendix E for illustration. A graphical display, comparing the observed data and model predictions, is given in Figures 5 through 8.

There were six aqueous phase response pulse tests (run numbers PW-3, PW-4, PW-6, PW-14, PW-22, and PW-24) in which adequate fitting of the model was not obtained. The reason may have been due to unusual topology of the response surface, ϕ', that could possibly be overcome if an exhaustive range of initial parameter estimates were tried. However, it is hardly coincidental that the ratio Q_B/Q_A is considerably less than 1 for all of these pulse tests (see Table 6). It was previously stated that the best fits for the 19 other data sets were with $Q_B/Q_A > 1$. The extraction factor mQ_B/Q_A, rather than the ratio Q_B/Q_A, is most likely the significant factor affecting the fitting of the model. The equations for the overall heights of a transfer unit (47) can be stated as

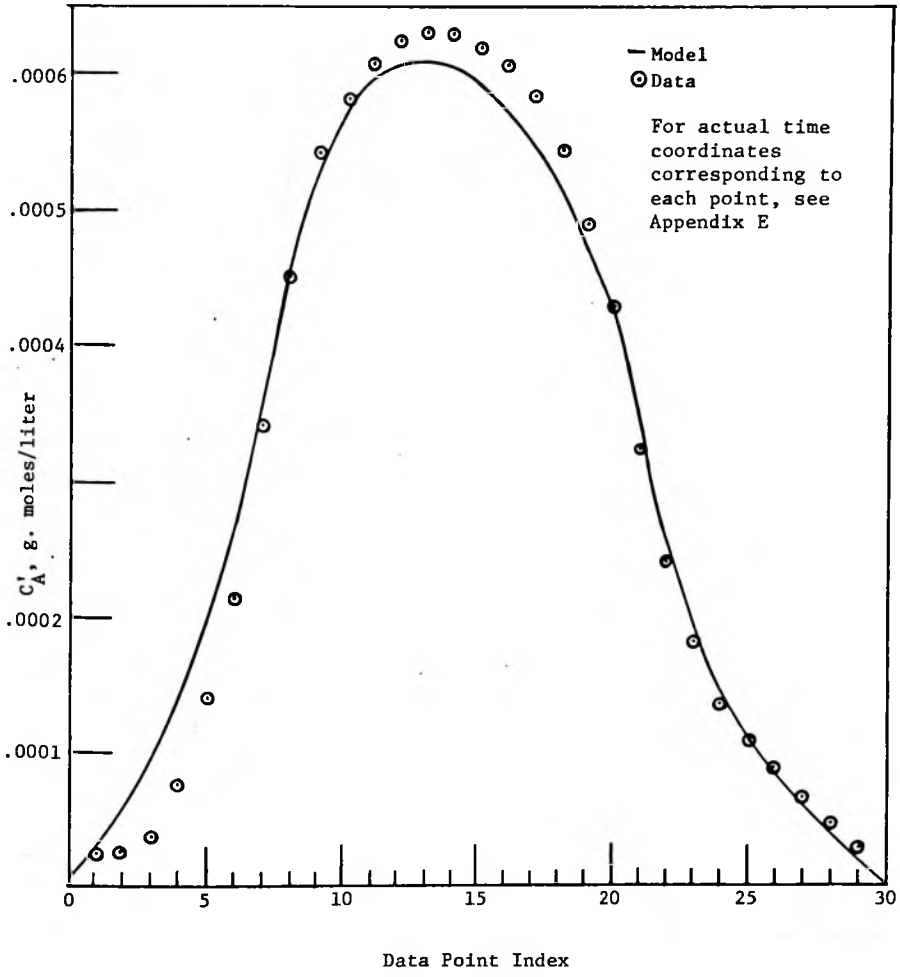

Figure 5. Comparison of Inverted Aqueous Phase Model and Experimental Data, Run PW-10

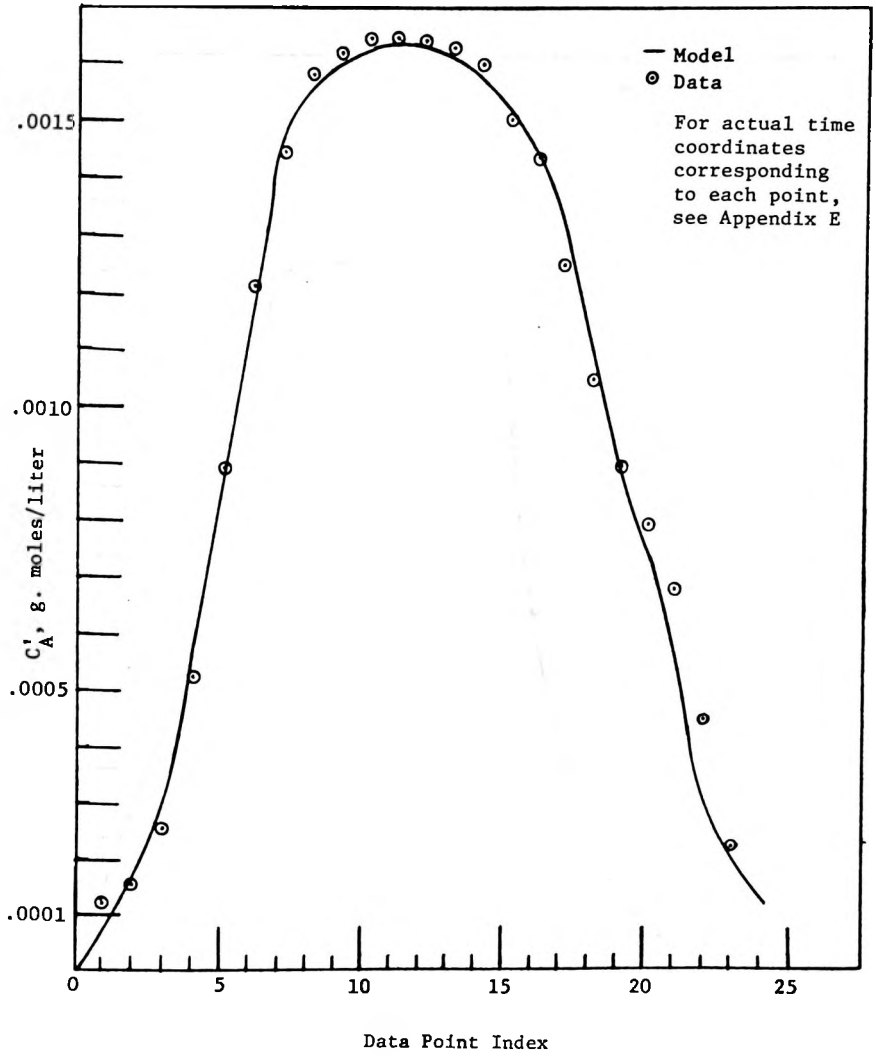

Figure 6. Comparison of Inverted Aqueous Phase Model and Experimental Data, Run PW-12

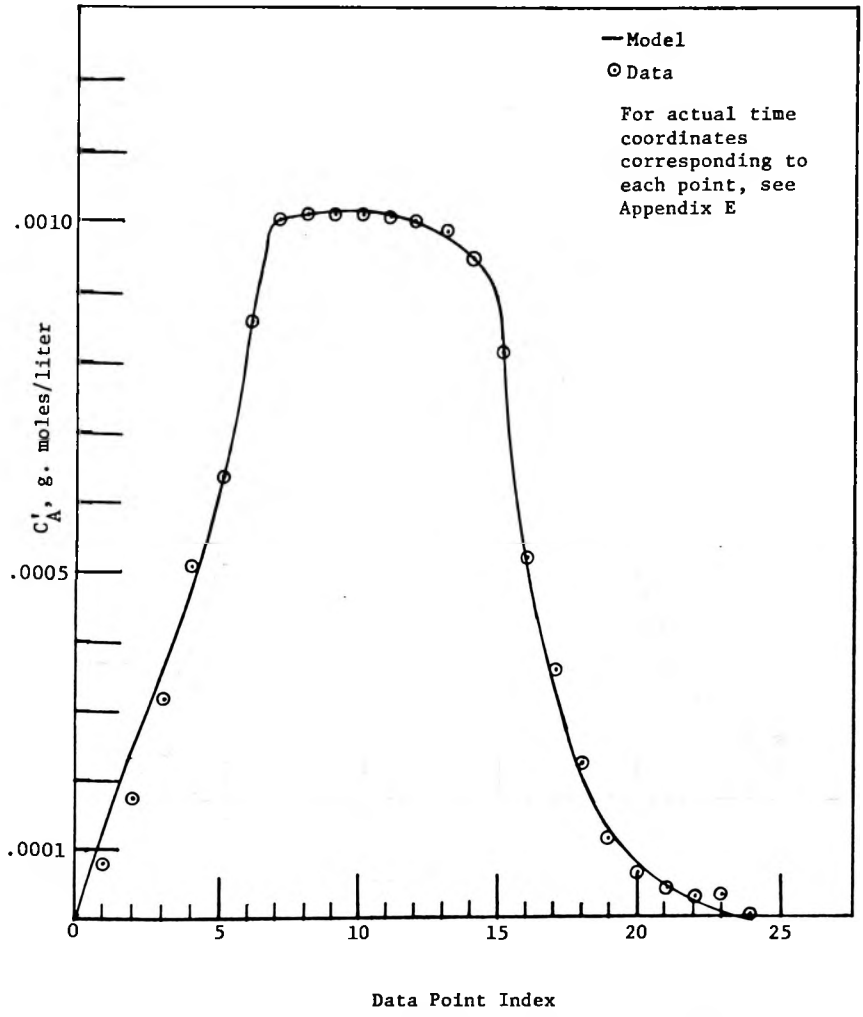

Figure 7. Comparison of Inverted Aqueous Phase Model and Experimental Data, Run PW-16

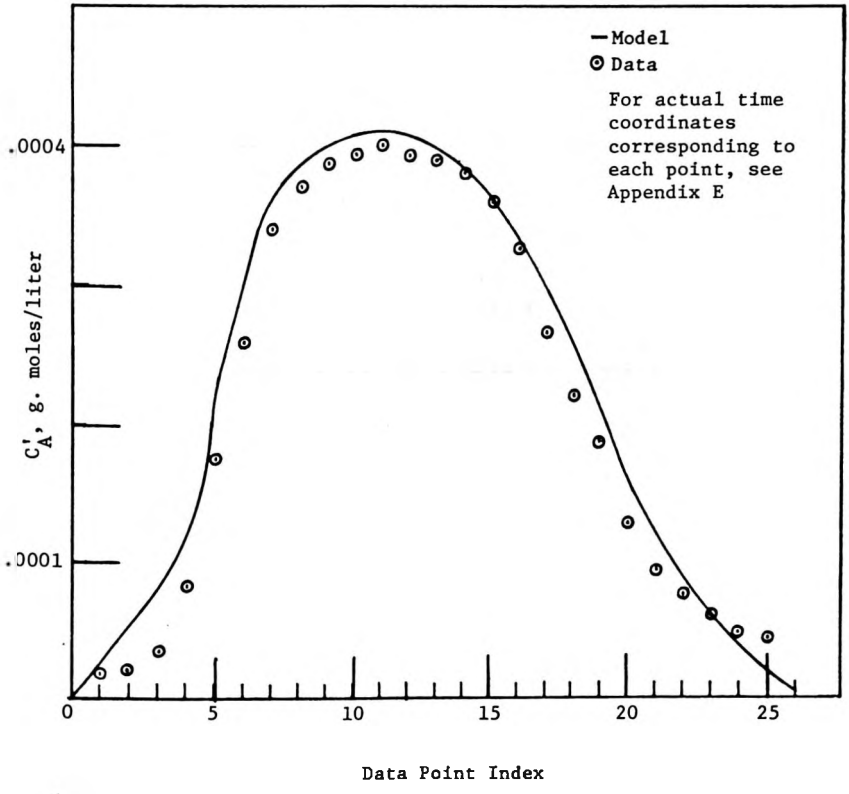

Figure 8. Comparison of Inverted Aqueous Phase Model and Experimental Data, Run PW-20

Table 6

Very-Difficult-To-Fit Pulse Tests
and Their Operating Conditions

Test No.	Q_A (cm/sec)	Q_B (cm/sec)	mQ_B/Q_A
PW-3	13.93	6.15	.231
PW-4	13.92	6.95	.262
PW-6	9.28	6.15	.348
PW-14	13.93	12.60	.475
PW-22	7.95	5.38	.355
PW-24	7.58	5.02	.348

$$H_{oB} = H_B + (mQ_B/Q_A)H_A \tag{137}$$

and

$$H_{oA} = H_A + (Q_A/mQ_B)H_B. \tag{138}$$

One can see from Equations 137 and 138 that large values of the extraction factor (mQ_B/Q_A) increase the significance of the aqueous phase resistance and reduce the significance of the organic phase resistance. If one plots H_{oB} versus mQ_B/Q_A for the seven best fits (Figure 9) one can see a positive slope trend that is indicative of the behavior of Equation 137 if changes in H_B and H_A are negligible. The other 12 fits, mostly at low values of extraction factor, show scatter for changes in mQ_B/Q_A, and are not shown in Figure 9. The increased scatter at low values of extraction factor is an indication that H_B variability is increasingly significant in the overall resistance to mass transfer for small extraction factors. An estimate of the individual resistances can be obtained from the slope and intercept of Figure 9; the slope is H_A and the intercept is H_B. From Figure 9, the dispersed phase resistance, H_B, = .018 ft., and the continuous phase resistance, H_A, = .461 ft. for large extraction factors in the system studied. Usually one cannot separate the overall resistance into individual resistances in solvent extraction by the above method, since the H_{oB} versus mQ_B/Q_A line tends to curve near the intercept. However, for purposes of comparing the relative values of H_B and H_A with each other, the technique is used here. The assumption of linearity may be more valid in this study also, since the values of H_{oB} are so small.

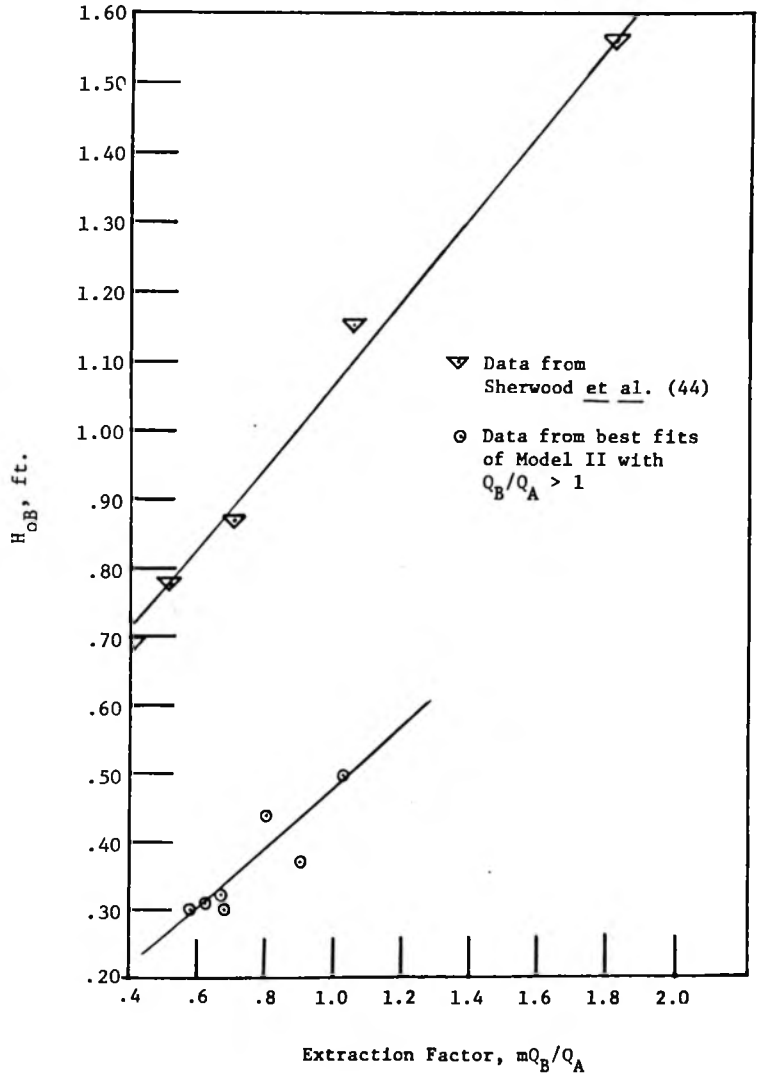

Figure 9. Overall HTU's and Large Extraction Factors

Figure 9 also shows, for comparative purposes, a plot of data from Sherwood et al. (44). One can see, by comparing slopes, that Sherwood's individual aqueous phase resistance, H_A, was in the same range as that obtained in this study, but by noting the contrasting intercepts of the two lines representing the two data sets, it is concluded that their individual dispersed phase resistance, H_B, was much larger than the average H_B in this investigation. The differences in the dispersed phase resistance, H_B, may be due to the fact that the packing used by Sherwood et al. was 1/2 inch rings, compared with 3/8 inch rings used in this study. Larger packing would tend to reduce the dispersed phase holdup and interfacial area, thereby increasing dispersed phase resistance to mass transfer. Note also that Sherwood's data deviate slightly less from the linear relationship diagrammed in Figure 9. This does not necessarily indicate that his data are more accurate, but it does imply that the variabilities of the individual resistances, H_A and H_B, were less over the range of his steady state studies in comparison with the data from the dynamic pulse tests analyzed in this thesis.

Most previous investigators such as Treybal (48) and Sherwood and Pigford (45) have recommended large values of extraction factor to increase extraction efficiency. This recommendation is supported here, since the 19 data sets show higher mass transfer coefficients for increasing values of the ratio Q_B/Q_A. Since the value of $m = .525$ for the liquid system under study is relatively low, the importance of maintaining high Q_B/Q_A ratios may be more important here than for other systems. It would be interesting to study other liquid systems with

values of the distribution coefficient different than .525 to see if the significance of the effect or the sensitivity of the model to the ratio of Q_B and Q_A is altered.

There is a possibility that the assumption of plug flow in the organic phase for a packed column is not valid when Q_A is significantly greater than Q_B. One can also postulate that reduced mass transfer resistance in the discontinuous phase caused by maintaining large extraction factors increases the applicability of the model. Additional study in this area should clarify whether or not it is (1) a limitation of the model or (2) bad data or (3) unusual response surface topology that caused the difficulty in fitting the model for $Q_B/Q_A < 1$.

Packed Column--Organic Phase

Six organic phase data sets from pulse tests, whose aqueous response $G_A(1,jw)$ was previously evaluated, were fitted to $G_B(0,jw)$. The results are seen in Tables 5 and 6. A comparison of the aqueous phase and organic phase data fits (comparing Tables 2 and 3 with Tables 7 and 8) indicate that the organic phase fits were not as good as the aqueous phase fits when one compares values of ϕ'. One can also see that there is generally a poor comparison between estimated parameter values for the two phases. The mass transfer coefficients are smaller and the Peclet numbers much smaller for the organic phase response fits.

For additional comparison with data, the organic phase model solution was inverted into the time domain, using the parameters determined in the aqueous phase data fit. Then the predicted concentration versus time points computed from the model were superimposed upon

Table 7

Packed Column Organic Phase Fitted
Parameters and Operating Conditions

Test No.	k sec^{-1}	Pe_A	f_A	$\phi'(10^4)$	Q_A (cm^3/sec)	Q_B (cm^3/sec)	mQ_B/Q_A
PM-10	.00777	5.500	.300	4.193	9.94	15.15	.800
PM-11	.00250	0.323	.730	13.580	14.08	16.90	.631
PM-16	.00486	7.678	.652	5.518	9.87	10.85	.578
PM-20	.00196	0.213	.646	7.220	7.63	12.80	.881
PM-21	.00260	4.712	.702	8.385	8.12	9.90	.640
PM-23	.01010	2.010	.501	8.047	7.82	15.40	1.032

Table 8

Packed Column Organic Phase Fitted Parameters

Test No.	N_B	H_{oB} (ft)	h_{A_2} (cm^2)	h_{B_2} (cm^2)	θ_A (sec)	θ_B (sec)
PM-10	2.23	2.52	7.59	17.72	131	201
PM-11	0.641	8.78	18.50	6.81	225	69
PM-16	1.94	2.90	16.50	8.81	288	140
PM-20	0.663	8.49	16.60	8.71	374	116
PM-21	1.14	4.94	17.80	7.51	376	130
PM-23	2.84	1.98	12.70	12.61	279	130

the organic phase data pulse curve. The results for a representative organic phase data set are shown in Figure 10. One can see that a cyclic pattern resembling an underdamped oscillation appears to be the nature of the organic response model using parameters from the aqueous phase fit. The predicted and observed curves do generally agree near the peak and the tail of the observed curve. The cyclic nature of the predicted curve (if, perchance, it were the true response) would be most difficult to observe with the existing experimental system, where finite sample volumes were collected at time intervals and titrated. It would be particularly difficult to monitor the initial portion of the organic pulse curves by sample collection if the predicted large amplitudes and high frequency cycles were truly characteristic of the system during this period.

A least squares fit of the organic response, inverted into the time domain, is shown in Figure 11. If one compares the inverted organic response of the fitted model with the inverted organic response using aqueous phase response parameters, one can observe that the lower Peclet numbers of the fitted model alter the characteristic shape of the response curve, tending to produce a smoother pulse curve. The marked difference between fitted organic phase models and the inverted organic response using aqueous phase response parameters was typical for the other five organic phase pulse responses examined, also.

It should be noted that there was considerable uncertainty concerning when to terminate the tail of the organic phase pulse, since the concentrations (measured by titrating) were not significantly greater than the experimental error in the tailing portion of the data. One can therefore not positively determine whether the organic phase model equations, evaluated at the parameters obtained from least squares fits

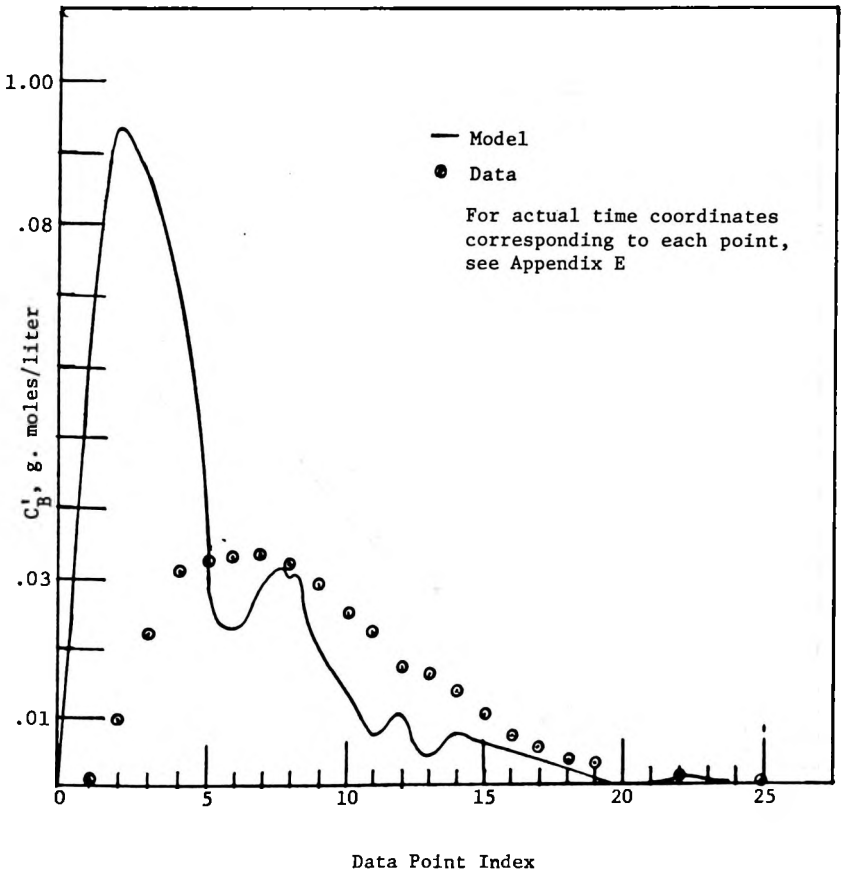

Figure 10. Comparison of Inverted Organic Phase Model and Experimental Data Using Aqueous Phase Transfer Function Parameters, Run PM-10

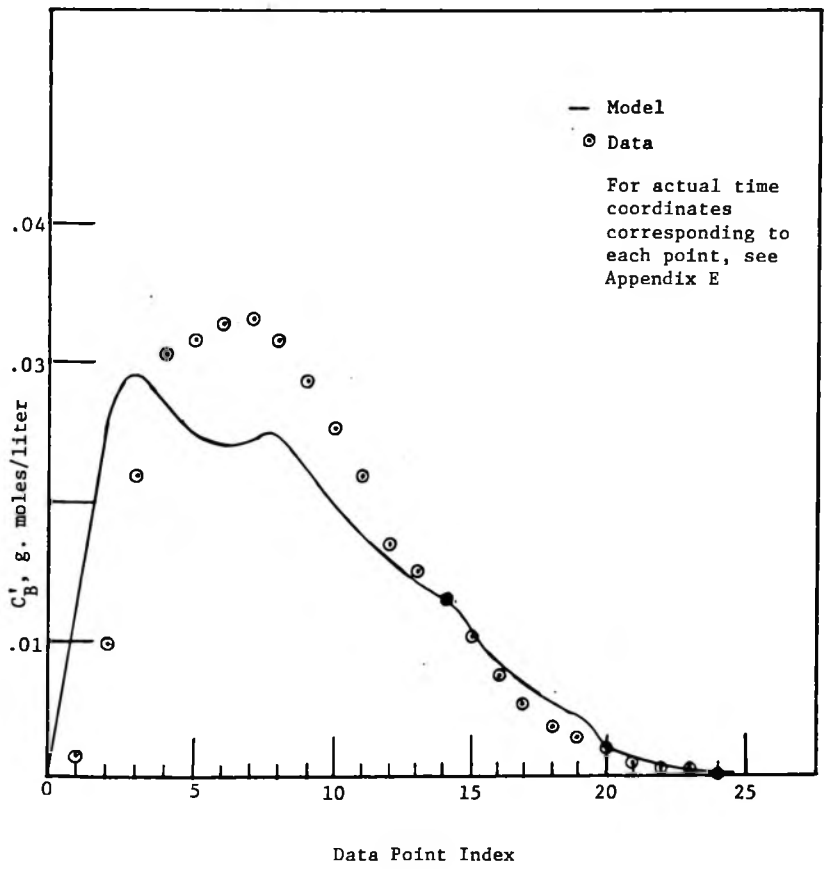

Figure 11. Comparison of Inverted Organic Phase Model and Experimental Data Using Organic Phase Transfer Function Parameters, Run PM-10

of aqueous phase data, are representative of the dispersed phase dynamics, because of uncertainties in the measuring technique. Additional testing, using a method of continuously recording the organic phase acid concentration, would be needed to clarify the above points and to obtain more definite conclusions concerning the modeling of the organic phase response.

Spray Column--Aqueous Phase

Five representative data sets were fitted to the aqueous phase transfer function equation giving $G_{AN}(1,jw)$ for the spray tower operation. See Tables 9 and 10 for representative spray column parameter values. A comparison with packed column parameters (Tables 2 and 3) is given below.

The Peclet numbers for the five representative spray column pulse tests range from 1.5 to 8.5, very much smaller in value than those estimated for the packed column, indicating much more axial dispersion in the spray column. These results agreed with the previously-reported observation (4,17) that axial dispersion is excessive in a spray column, and is one of the major reasons that industrial use of the spray column in extractive systems has been limited in recent years. However, the spray column still has economic advantages for dirty liquids (or those containing dispersed solids), and when extraction efficiency is not too important.

The spray column mass transfer coefficients are much smaller than those for the packed column operation, ranging from .00046 to .0056 sec^{-1} in the spray tower operation (except for run SW-17, discussed below). These coefficients are not small because of the lower Peclet

Table 9

Spray Column Aqueous Phase Fitted
Parameters and Operating Conditions

Test No.	k sec^{-1}	Pe_A	f_A	$\phi'(10^4)$	Q_A (cm^3/sec)	Q_B (cm^3/sec)	mQ_B/Q_A
SW-9	.000458	6.94	.850	1.4889	14.55	16.67	.601
SW-7	.00565	1.69	.927	1.6932	13.13	17.98	.718
SW-23	.00257	4.64	.978	2.1172	14.25	16.8	.620
SW-14	.000654	1.51	.922	.9365	9.6	12.1	.660
SW-17	.0000463	8.52	.607	.00148	14.1	10.55	.392

Table 10

Spray Column Aqueous Phase Fitted Parameters

Test No.	N_B	H_{oB} (ft)	h_{A_2} (cm^2)	h_{B_2} (cm^2)	θ_A (sec)	θ_B (sec)
SW-7	2.460	2.29	42.4	3.2	552	31
SW-9	0.216	26.2	38.8	6.8	457	70
SW-14	0.423	13.3	42.0	3.6	750	51
SW-17	0.035	159.0	27.7	17.9	337	200
SW-23	1.54	3.66	44.6	1.0	536	10

numbers of the spray tower, since, at least in theory, the coefficients are corrected for dispersion effects by use of the dispersion model in their determination. Rather, the low values of the mass transfer coefficients reported in Table 9 are probably due to inadequate interfacial area available for mass transfer, as indicated by low values of organic phase holdup, h_B, or high values of f_A and resultant low organic phase residence time θ_B. The fractional organic holdup $(1-f_A)$, for example, is .363 for packed column test PW-11 and .150 for spray column test SW-9, both having comparable volumetric phase flow rates; similarly, $(1-f_A)$ = .437 for PW-16 and $(1-f_A)$ = .078 for SW-14, again at comparable phase flow rates.

One should keep in mind that the rate of mass transfer is much more dependent on the drop formation characteristics in a spray tower operation than for a packed column. For a packed column, the packing characteristics are more important than the drop size characteristics of the dispersed phase. Burge (4) discussed the drop formation characteristics of a spray tower operation, and noted that, in the range of flow rates between 10 to 12 cm^3/sec., the discontinuous phase of a spray tower is in a transition state from unhindered upward droplet movement to a state of continuous collision and coalescing of the drops. This transition results in marked changes in the axial dispersion characteristics of the phases. Since the volumetric flow rate of the organic phase in run SW-17 is in the range of this transition state, one might conclude that the very low mass transfer coefficient (.000046 $sec.^{-1}$) and low f_A(.607) were due to interfacial area instability caused by transition of the droplet formation

to a new type of discontinuous phase flow pattern, and hence is not characteristic of general spray tower operations outside of the transition range.

CHAPTER IX

RECOMMENDATIONS

Based on the previously-discussed data analysis, additional study to clarify the aqueous phase model's applicability with regard to the extraction factor should be explored further. A good area of research would be to test the model for systems having comparatively large extraction factors, in addition to a large distribution factor, m, but with $Q_B/Q_A < 1$. Such exploratory study should confirm whether or not the model's performance is dependent on the relative significance of the organic phase's resistance to mass transfer, as concluded in Chapter VIII. If this tentative conclusion is proved invalid by further testing, then the assumption of plug flow in the discontinuous phase for $Q_B/Q_A < 1$ is suspect, and the dispersive mechanism should be used to describe discontinuous phase mixing. Experimental comparisons of the interfacial area per unit volume as determined by conventional methods and by parameter estimations using the dispersion model, would also be a good subject for future investigations.

It was reported in Chapter VIII that the dispersion model, when used to derive the discontinuous (organic) phase transfer function, predicts a time domain response whose shape is highly variable, depending on the degree of dispersion. Attempts should be made to develop a nearly instantaneous concentration measurement for the organic phase (in place of the conventional averaged concentration measurements

obtained using analysis of intermittent samples) to determine whether the previously-described cyclic response actually occurs in an extraction column.

Studies of the model using optimum-seeking algorithms to find the best combination of transfer coefficients, phase holdups, Peclet numbers and phase rates (not all independent, of course) to achieve maximum yield in the extract phase at minimum cost would be a useful purpose for the model that was developed in this study.

Frequency domain modeling of the general unsteady state model derived in Chapter III would also be an area of commendable and worthwhile study, if the mathematical techniques needed to obtain the frequency domain solution can be developed.

BIBLIOGRAPHY

1. Ballard, J. H. and Piret, E. L., Ind. Eng. Chem. 38, 1088 (1950).

2. Brittan, M. J., Chem. Eng. Sci. 22, 1019 (1967).

3. Brutvan, D. R., Ph.D. Dissertation, Rensselaer Polytechnic Institute, 1958.

4. Burge, D. A., "Characterization of Axial Mixing in a Spray Column," M.S. Thesis, University of Alabama, 1969.

5. Clements, W. C., Jr., "Part I. An Investigation of Computational Methods and Difficulties in Pulse Testing" and "Part II. Application of Pulse Testing to Flow and Extraction Dynamics," Ph.D. Thesis, Vanderbilt University, 1963.

6. Clements, W. C., Jr., Chem. Eng. Sci. 24, 957 (1969).

7. Clements, W. C., Jr., and Schnelle, K. B., Jr., Ind. Eng. Chem. Proc. Des. and Dev. 2, 94 (1963).

8. Clements, W. C., Jr., Inst. & Cont. Syst. 41, 97 (Nov. 1968).

9. Clements, W. C., Jr., Personal Communication, 1970.

10. Clements, W. C., Jr., "Numerical Transformation of a Single Time Pulse," University of Alabama, Department of Chemical Engineering, 1967 (Computer Program Description).

11. Clements, W. C., Jr., Lecture Notes, CHE 300, "Mathematical Modeling," University of Alabama, 1969.

12. Clements, W. C., Jr., "Description of a Computer Program for Frequency Domain Modeling of Mathematical Models for Dynamic Systems," University of Alabama, Department of Chemical and Metallurgical Engineering, 1969.

13. Danckwerts, P. W., Chem. Eng. Sci. 2, 1 (1953).

14. Daniels, F., Williams, J. W., Bender, P., Alberty, R. A., and Cornwell, C. D., Experimental Physical Chemistry, New York: McGraw-Hill Book Company, 1962.

15. Davies, O. L., Design and Analysis of Industrial Experiments, Edinburgh, Scotland: Oliver and Boyd, 1954.

16. Doninger, J. E. and Stevens, W. F., A.I.Ch.E. Journal 14, 591 (1968).

17. Elkins, L. O., "Steady State and Dynamic Analyses of Continuous Countercurrent Liquid-Liquid Extraction Columns," Ph.D. Thesis, Vanderbilt University, 1966.

18. Fan, L. T. and Ahn, Y. K., C.E.P. Symposium Series 46, 91 (1963).

19. Garner, F. H. and Hale, A. R., J. Appl. Chem. 5, 653 (1953).

20. Geankoplis, C. J. and Hixon, A. N., Ind. Eng. Chem. 42, 1141 (1950).

21. Gray, R. T., "The Dynamics of a Packed Gas Absorber by Frequency Response Analysis," Ph.D. Thesis, University of Tennessee, 1961.

22. Hartley, H. O., Technometrics 3, 269 (1961).

23. Hays, J. R., Clements, W. C., Jr., and Harris, T. R., A.I.Ch.E. Journal 13, 374 (1967).

24. Hazelbeck, D. E. and Geankoplis, C. J., Ind. Eng. Chem. Fundamentals 2, 310 (1963).

25. Jeffreson, C. P., Chem. Eng. Sci. 25, 1319 (1970).

26. Justice, R. G., "Frequency Response of Single Phase Longitudinal Dispersion and Two Phase Extraction in Packed Beds Using Pulse Testing Methods," Ph.D. Thesis, Vanderbilt University, 1963.

27. Karr, A. E. and Scheibel, E. G., C.E.P. Symposium Series 50, 73 (1954).

28. Levenspiel, O. and Bischoff, K. B., Ind. Eng. Chem. 51, 1431 (1959).

29. Lewis, J. B., Chem. Eng. Sci. 8, 295 (1958).

30. Li, N. N. and Ziegler, E. N., Ind. Eng. Chem. 59, 30 (1967).

31. Marquardt, D. W., Chem. Eng. Prog. 55, 65 (1959).

32. Marquardt, D. W., J. Soc. Ind. Appl. Math. 11, 431 (1963).

33. Mecklenburgh, J. C. and Hartland, S., Can. J. Chem. Eng. 47, 453 (1969).

34. Miyauchi, T. and Vermeulen, T., Ind. Eng. Chem. Fundamentals 2, 113 (1963).

35. Miyauchi, T. and Vermeulen, T., Ind. Eng. Chem. Fundamentals 2, 304 (1963).

36. Muller, D. E., Math Tables Aids Comput. 10, 208 (1956).

37. Pollock, G. G. and Johnson, A. I., Can. J. Chem. Eng. 47, 469 (1969).

38. Pollock, G. G. and Johnson, A. I., Can. J. Chem. Eng. 47, 565 (1969).

39. Pollock, G. G. and Johnson, A. I., Can. J. Chem. Eng. 48, 64 (1970).

40. Ralston, A. and Wilf, H. S., Mathematical Methods for Digital Computers, Volume II, New York: Wiley, 1967.

41. Sater, V. E. and Levenspiel, O., Ind. Eng. Chem. Fund. 5, 86 (1966).

42. Scheibel, E. G. and Karr, A. E., Ind. Eng. Chem. 42, 1048 (1950).

43. Sheridan, S. H., "A Study of Longitudinal Dispersion in Straight Pipes," M.S. Thesis, University of Alabama, 1968.

44. Sherwood, T. K., Evans, J. E., and Longcor, J. V. A., Ind. Eng. Chem. 31, 1144 (1939).

45. Sherwood, T. K. and Pigford, R. L., Absorption and Extraction, New York: McGraw-Hill Book Company, 1952.

46. Sleicher, C. A., Jr., A.I.Ch.E. Journal 5, 145 (1959).

47. Treybal, R. E., Mass Transfer Operations, New York: McGraw-Hill Book Company, 1968.

48. Treybal, R. E., Liquid Extraction, New York: McGraw-Hill Book Company, 1963.

49. Vermeulen, T., Moon, J. S., Hennico, A. and Miyauchi, T., Chem. Eng. Prog. 62, 95 (1966).

50. Wehner, J. F. and Wilhelm, R. H., Chem. Eng. Sci. 6, 89 (1956).

51. Whitman, W. G., Chem. & Met. Eng. 29, 147 (1923).

52. Williams, J. A. and Adler, R. J., Ind. Eng. Chem. Fund. 9, 193 (1970).

53. Zenz, F. A., Petrol. Refiner 36, 147 (1957).

TABLE OF NOMENCLATURE

a	Specific interfacial area per unit of active extractive volume, 1/L
a_1	Complex variable defined in Equation 20
a_2	Complex variable defined in Equation 21
A_1, A_2, A_3	Complex coefficients of the frequency domain solution to the third degree characteristic equation, Equation 28
A_{1s}, A_{2s}, A_{3s}	Steady state coefficients of the frequency domain solution to the steady state characteristic equation, Equation 39
A_1'	Coefficient defined in Equation 79
A_{2s}'	Coefficient defined in Equation 73
$\underline{A}_i$	Constant in parabolic line segment equation used to approximate time functions
$\underline{A}_i'$	Constant in parabolic line segment equation used to approximate F(jw)
B_1, B_2, B_3	Coefficients of the Laplace domain solution to the third degree characteristic equation, Equation 28
$\underline{B}_i$	Constant in parabolic line segment equation used to approximate f(t)
$\underline{B}_i'$	Constant in parabolic line segment equation used to approximate F(jw)
C_1 through C_7	Real coefficients shown in Equation 44
C_A	Dimensionless concentration of aqueous phase
C_B	Dimensionless concentration of organic phase
$\underline{C}_A$	Concentration of the aqueous phase, M/L^3
$\underline{C}_B^*$	Equilibrium concentration of organic phase, M/L^3

C'_A	Concentration of aqueous phase, deviation from steady state, M/L^3
C'_B	Concentration of organic phase, deviation from steady state, M/L^3
$\bar{C}_A$	Laplace transform with respect to time of the aqueous phase concentration variable, M/L^3
$\bar{C}_B$	Laplace transform with respect to time of the organic phase concentration variable, M/L^3
$\bar{C}_{in}$	Laplace transform with respect to time of the aqueous feed concentration, M/L^3
$\bar{\bar{C}}_A$	Laplace transform with respect to time and Z of the aqueous phase concentration variable, M/L^3
$\bar{\bar{C}}_B$	Laplace transform with respect to time and Z of the organic phase concentration variable, M/L^3
$\underline{C}_i$	Constant in parabolic line segment equation used to approximate f(t)
$\underline{C}'_i$	Constant in parabolic line segment equation used to approximate F(jw)
C_{ref}	Reference concentration, M/L^3
d	Coefficient in Equation 29
d_s	Steady state coefficient in Equation 39
d_p	Dispersed phase drop diameter, L
d_R	Real part of coefficient d defined in Equation 29
d_I	Imaginary part of coefficient d defined in Equation 29
d_{FC}	Minimum critical packing size defined in Equation 85, L
D_A	Dispersion coefficient of aqueous phase, L^2/T
D_B	Dispersion coefficient of organic phase, L^2/T
D_1 through D_5	Coefficients in Equation 45

e	Coefficient defined in Equation 30
e_s	Steady state coefficient in Equation 39
$e(t)$	Error between observed and predicted time function, $y_o(t) - y_p(t)$
$E(jw)$	Fourier transform of e(t)
f	Coefficient defined in Equation 31
f_A	Fractional aqueous holdup = $h_A/S\varepsilon$ (dimensionless)
$f(t)$	Time function in Fourier transform operations
$F(q)$	Function defined in Equation 28
$F^*(q)$	Function formed by replacing all the coefficients of F(q) with their conjugates
$F(m^{(o)})$ $F(m^{(1)})$ $F(m^{(2)})$	Calculated values of left side of Equation 28 for trial roots $m^{(o)}$, $m^{(1)}$, $m^{(2)}$ in Muller method for finding roots
$F_2(q)$	Quadratic function defined in Equation 43
$F_4(q)$	Fourth degree function defined in Equation 45
$F_6(q)$	Sixth degree function defined in Equation 44
$F(jw)$	Fourier transform of f(t)
g	Acceleration due to gravity, L/T^2
G_A	Aqueous phase concentration transfer function, equal to $\overline{C}_A(1,jw)/\overline{C}_{in}(0,jw)$
G_B	Organic phase concentration transfer function, equal to $\overline{C}_B(0,jw)/\overline{C}_{in}(0,jw)$
G_{AN}	Normalized aqueous phase concentration transfer function, equal to $[\overline{C}_A(1,jw)/\overline{C}_A(1,0)]/[\overline{C}_{in}(0,jw)/\overline{C}_{in}(0,0)]$
G_{BN}	Normalized organic phase concentration transfer function, equal to $[\overline{C}_B(0,jw)/\overline{C}_B(0,0)]/[\overline{C}_{in}(0,jw)/\overline{C}_{in}(0,0)]$
$G_o(jw)$	Frequency response function computed from a dynamic test, equal to $Y_o(jw)/X_o(jw)$

$G_p(jw)$	Frequency response function predicted from a model solution, equal to $Y_p(jw)/X(jw)$
h_A	Holdup of aqueous phase per unit length of column, L^2
h_B	Holdup of organic phase per unit length of column, L^2
H	Real coefficient in Equation 43
H_{oB}	Overall height of a transfer unit based on dispersed (organic) phase, L
H_A	Individual height of a transfer unit, based on continuous (aqueous) phase, L
H_B	Individual height of a transfer unit, based on dispersed (organic) phase, L
i	Counting integer
I(w)	Imaginary part of Fourier transform
$I_o(w)$	Imaginary part of $Y_o(jw)$
$I_p(w)$	Imaginary part of $Y_p(jw)$
j	$(-1)^{1/2}$
J	Real coefficient in Equation 43
k	Overall mass transfer coefficient, equal to $K_B a$,1/T
K_B	Overall mass transfer coefficient based on organic phase, L/T
K_{cs}	Cell constant for Leeds and Northrup standard electrical conductivity cell, 1/L
K_{cf}	Cell constant for electrical conductivity cell used in dynamic testing, 1/L
L	Length of column, L
L_c	Measured conductance, mhos
L_s	Specific conductance of solution being measured, mhos/L
L_{cf}	Measured conductance of experimentally determined conductivity cell, mhos

L_{cs}	Measured conductance of standard electrical conductivity cell, mhos
m	Slope of equilibrium line
m_1, m_2, m_3	Frequency domain roots of the third degree characteristic equation defined in Equation 28
m_{1s} m_{2s} m_{3s}	Steady state frequency domain roots of the third degree steady state characteristic equation, Equation 39
m_{R1} m_{R2} m_{R3}	Real parts of m_1, m_2, m_3, respectively
m_{I1} m_{I2} m_{I3}	Imaginary parts of m_1, m_2, m_3, respectively
m_1', m_2', m_3'	Laplace domain roots of the third degree characteristic equation defined in Equation 28
$m^{(o)}$, $m^{(1)}$, $m^{(2)}$, $m^{(3)}$	Trial roots in Muller method for finding roots
M	Transducer millivolt output signal
n	Number of data points
N_A	Number of aqueous phase transfer units, $kS\varepsilon L/Q_A$ (dimensionless)
N_B	Number of organic phase transfer units, $kS\varepsilon L/Q_B$
P_1, P_2, P_3, P_4	Laplace domain roots of the fourth degree characteristic equation defined in Equation 19
P_1, P_2, P_3, P_4	Coefficients of the Laplace domain solution to the fourth degree equation, Equation 19
Pe_A	Dimensionless aqueous phase Peclet number, equal to LQ_A/D_Ah_A
Pe_B	Dimensionless organic phase Peclet number, equal to LQ_B/D_Bh_B

q	Independent variable of the Laplace transform with respect to Z, 1/L
Q_A	Volumetric flow rate of aqueous phase, L^3/T
Q_B	Volumetric flow rate of organic phase, L^3/T
r_1, r_2	Coefficients in Equation 46
$R(q)$	Remainder factor defined in Equation 46
R_s	Series resistance in electrical conductivity transducer
R_{cf}	Reciprocal of L_{cf}, ohms
$R(w)$	Real part of Fourier transform
R_i	Difference between y_{oi} and y_{poi}
$R_o(w)$	Real part of $Y_o(jw)$
$R_p(w)$	Real part of $Y_p(jw)$
s	Independent variable of the Laplace transform with respect to time, 1/T
S	Cross-sectional area of column, L^2
t	Time, T
T_i	Time point between parabolic line segments
u	Parameter of example model in Chapter VII
$\underline{u}(t-T_i)$	Step function occurring at time T_i
u_o	Initial estimate of parameter u
u_1	Corrected parameter estimate given by Equation 112
U_i	Parameter defined in Equation 103
v	Parameter of example model in Chapter VII
v_o	Initial estimate of parameter v
v_1	Corrected parameter estimate given by Equation 113
V_i	Parameter defined in Equation 104
w	Radian frequency, radians per unit time

W_i	Frequency point at intersection of parabolic line segments
x	Length coordinate, L
X(jw)	Fourier transform of arbitrary forcing function
$X_o(jw)$	Fourier transform of observed input response
y_{oi}	Observed time domain response at data point i
$y_o(t)$	Observed time domain response
$y_p(t)$	Predicted time domain response
y_{poi}	Predicted time domain response for data point i, defined in Equation 105
y_{pi}	Predicted time domain response for data point i, defined in Equation 106
$Y_o(jw)$	Fourier transform of $y_o(t)$
$Y_p(jw)$	Fourier transform of $y_p(t)$
Z	Dimensionless length variable, X/L

Greek Letters

α_o through α_5	Coefficients in polynomial used to correlate L_{cf} and M
ΔI	$I_o(w) - I_p(w)$
ΔR	$R_o(w) - R_p(w)$
Δu	Correction for new estimate of u
Δv	Correction for new estimate of v
$\Delta\rho$	Absolute value of difference in density of aqueous phase and organic phase, M/L^3
ϵ	Fractional void volume = 1 for spray column and < 1 for packed column (dimensionless)
ϕ	Sum of squared error
ϕ_o	Initial sum of squared error
ϕ_1	Sum of squared error after correction of parameter estimates
ϕ'	Integral square error
σ	Interfacial tension shown in Equation 85, M/T^2
θ_A	Aqueous phase residence time, $h_A L/Q_A$
θ_B	Organic phase residence time, $h_B L/Q_B$

APPENDIX A

DETERMINATION OF DISTRIBUTION COEFFICIENT

The distribution coefficient, m, was computed from the data shown in Table A1.

Table A1

Equilibrium Data From Scheibel and Karr (42)

Methyl Isobutyl Ketone -- Acetic Acid -- Water

28°C

$\underline{C}_A$ g. mole/liter	$\underline{C}_B^*$ g. mole/liter
.1569	.0772
.233	.1155
.482	.244
.733	.380

A linear least squares fit of the above data yields:

$$\underline{C}_B^* = -0.00663 + .525\ \underline{C}_A$$

with Standard Error of Estimate = .00236 g. mole/liter

Correlation Coefficient = .9999

A comparison of the predicted and observed equilibrium organic phase concentrations is tabulated in Table A2 below.

Table A2

Comparison of Observed and Predicted
Equilibrium Organic Phase Concentrations

	Observed	Predicted
C_A, g. mole/liter	C_B^*, g. Mole/liter	C_B^*, g. mole/liter
.1569	.0772	.0758
.233	.1155	.1157
.482	.244	.247
.733	.380	.378

Although the above correlation used data at 28°C, Justice (26) found that the temperature sensitivity of the distribution coefficient, m, for the methyl isobutyl ketone -- acetic acid -- water system is minimal over the range of temperature that is applicable to this invetigation.

APPENDIX B

TRANSDUCER CALIBRATIONS

As discussed in Chapter IV and illustrated in Figure 4, a non-linear relationship between cell conductance L_{cf} and conductivity cell transducer millivolt output existed for the range of concentrations in the pulse tests. A series of polynomial least squares fits of $L_{cf}(10^4)$ versus millivolt output M from the transducers was made with the fitted polynomials ranging in degree from 2 to 8. Consequently, it was decided that a fifth degree polynomial fit reproduced the data very accurately for the range used in the experimentation.

The polynomial used in fitting the data was:

$$(10^4)L_{cf} = \alpha_o + \alpha_1 M + \alpha_2 M^2 + \alpha_3 M^3 + \alpha_4 M^4 + \alpha_5 M^5 \qquad (139)$$

The six estimated coefficients for each of the transducers used and the pulse tests for which the correlations are applicable are listed below.

#5 Transducer -- Spray Column Tests

Correlation Coefficient = .99990

Standard Error of Estimate = $.82298(10^{-3})$ mhos(10^{4})

Spray Column Pulse Tests:

SW-1 to SW-11

SW-24 to SW-27

$\alpha_o = + .73280(10^{-1})$

$\alpha_1 = + .128180$

$\alpha_2 = - .15957(10^{-1})$

$\alpha_3 = + .14217(10^{-2})$

$\alpha_4 = - .62257(10^{-4})$

$\alpha_5 = + .10407(10^{-5})$

#6 Transducer -- Spray Column Tests

Correlation Coefficient = .99995

Standard Error of Estimate = $.53256(10^{-3})$ mhos(10^{4})

Spray Column Pulse Tests:

SW-12 to SW-23

SW-28 to SW-36

$\alpha_o = + .81292(10^{-1})$

$\alpha_1 = + .10313$

$\alpha_2 = - .11113(10^{-1})$

$\alpha_3 = + .89663(10^{-3})$

$\alpha_4 = - .36323(10^{-4})$

$\alpha_5 = + .56794(10^{-6})$

#6 Transducer -- Packed Column Tests

Correlation Coefficient = .99993

Standard Error of Estimate = $.54906(10^{-3})$ mhos(10^{4})

Packed Column Pulse Tests:

PW-1 to PW-23

$\alpha_o = + .78855(10^{-1})$

$\alpha_1 = + .94665(10^{-1})$

$\alpha_2 = - .10093(10^{-1})$

$\alpha_3 = + .81953(10^{-3})$

$\alpha_4 = - .33556(10^{-4})$

$\alpha_5 = + .53146(10^{-6})$

#7 Transducer -- Packed Column Tests

Correlation Coefficient = .99991

Standard Error of Estimate = $.57487(10^{-3})$ mhos(10^{4})

Packed Column Pulse Tests:

PW-24 , PW-25

$\alpha_o = + .77602(10^{-1})$

$\alpha_1 = + .88551(10^{-1})$

$\alpha_2 = - .94452(10^{-2})$

$\alpha_3 = + .75527(10^{-3})$

$\alpha_4 = - .29826(10^{-4})$

$\alpha_5 = + .44895(10^{-6})$

APPENDIX C

SAMPLE PULSE TEST RESPONSE DATA

IDENTIFICATION PW-10

INPUT DATA

NUMBER OF TIME POINTS 31
INITIAL FREQUENCY 0.0
FREQUENCY INCREMENT 0.69999998E-03
FINAL FREQUENCY 0.20999998E-01
DEAD TIME 242.00000

t, sec. TIME	C_A', g. moles/liter PULSE ORDINATES
0.0	0.0
12.000000	0.23480708D-04
24.000000	0.25857051D-04
36.000000	0.39106511D-04
60.000000	0.75699936D-04
84.000000	0.13858185D-03
108.00000	0.21443538D-03
144.00000	0.34176395D-03
180.00000	0.45231497D-03
216.00000	0.54279249D-03
240.00000	0.58218697D-03
264.00000	0.60700485D-03
288.00000	0.62397984D-03
312.00000	0.63099386D-03
336.00000	0.63099386D-03
360.00000	0.62197750D-03
384.00000	0.60800067D-03
408.00000	0.58317650D-03
456.00000	0.54475432D-03
516.00000	0.48913155D-03
576.00000	0.42818114D-03
696.00000	0.32266602D-03
816.00000	0.23948451D-03
936.00000	0.17983114D-03
1056.0000	0.13347944D-03
1176.0000	0.10706957D-03
1296.0000	0.87559660D-04
1536.0000	0.63718864D-04
1776.0000	0.44993890D-04
2016.0000	0.28328330D-04
2256.0000	0.0

IDENTIFICATION PW-12

INPUT DATA

NUMBER OF TIME POINTS 25
INITIAL FREQUENCY 0.0
FREQUENCY INCREMENT 0.10700000E-02
FINAL FREQUENCY 0.31999998E-01
DEAD TIME 119.00000

t, sec. TIME	C_A', g. moles/liter PULSE ORDINATES
0.0	0.0
24.000000	0.11165703D-03
48.000000	0.14485657D-03
72.000000	0.25467901D-03
96.000000	0.52710134D-03
120.00000	0.89520961D-03
144.00000	0.12119131D-02
168.00000	0.14408522D-02
192.00000	0.15820577D-02
204.00000	0.16186053D-02
216.00000	0.16400185D-02
228.00000	0.16461485D-02
240.00000	0.16400185D-02
252.00000	0.16277726D-02
264.00000	0.15972618D-02
288.00000	0.15035740D-02
312.00000	0.14319359D-02
360.00000	0.12468514D-02
420.00000	0.10430261D-02
480.00000	0.89520961D-03
540.00000	0.79514598D-03
600.00000	0.67962054D-03
720.00000	0.45031914D-03
840.00000	0.22158604D-03
912.00000	0.0

IDENTIFICATION PW-16

INPUT DATA

NUMBER OF TIME POINTS 25
INITIAL FREQUENCY 0.0
FREQUENCY INCREMENT 0.73999981E-03
FINAL FREQUENCY 0.22200000E-01
DEAD TIME 224.00000

t, sec. TIME	C'_A, g. moles/liter PULSE ORDINATES
0.0	0.0
30.000000	0.78519792D-04
54.000000	0.17630379D-03
78.000000	0.31839381D-03
102.00000	0.51263883D-03
126.00000	0.63742418D-03
174.00000	0.86218258D-03
210.00000	0.10058568D-02
234.00000	0.10931580D-02
258.00000	0.11185671D-02
282.00000	0.11058371D-02
306.00000	0.10805295D-02
330.00000	0.10305392D-02
354.00000	0.98626548D-03
414.00000	0.85053989D-03
474.00000	0.71435049D-03
594.00000	0.51903585D-03
714.00000	0.36027771D-03
834.00000	0.22580006D-03
954.00000	0.11513090D-03
1074.0000	0.63413157D-04
1194.0000	0.43001826D-04
1314.0000	0.32262746D-04
1554.0000	0.31147050D-04
1794.0000	0.0

IDENTIFICATION PW-20

INPUT DATA

NUMBER OF TIME POINTS 27
INITIAL FREQUENCY 0.0
FREQUENCY INCREMENT 0.47999993E-03
FINAL FREQUENCY 0.14399998E-01
DEAD TIME 253.00000

t, sec. TIME	C'_A, g. moles/liter PULSE ORDINATES
0.0	0.0
24.000000	0.17544735D-04
48.000000	0.19970859D-04
84.000000	0.34015437D-04
132.00000	0.80964004D-04
192.00000	0.17317661D-03
252.00000	0.25934470D-03
312.00000	0.33898349D-03
348.00000	0.36929338D-03
384.00000	0.38716709D-03
420.00000	0.39253570D-03
456.00000	0.39790734D-03
492.00000	0.39253570D-03
528.00000	0.38716709D-03
564.00000	0.38001337D-03
624.00000	0.35858434D-03
684.00000	0.32653171D-03
804.00000	0.26461505D-03
924.00000	0.21923269D-03
1044.0000	0.18666768D-03
1224.0000	0.12745311D-03
1404.0000	0.90959205D-04
1584.0000	0.75410135D-04
1824.0000	0.56996374D-04
2064.0000	0.47286230D-04
2304.0000	0.41556879D-04
3012.0000	0.0

APPENDIX D

FOURIER TRANSFORMATION SAMPLE DATA

IDENTIFICATION PW-10

AREA UNDER PULSE = 0.44559881

RADIAN FREQUENCY	TRANSFORM MAGNITUDE	PHASE ANGLE (DEG)	PHASE ANGLE LESS DEAD TIME (DEG)	NORMALIZED MAGNITUDE
0.0	0.44559881	0.0	0.0	1.0000000
0.69999998D-03	0.42550110	-34.739227	-25.033325	0.95489731
0.14000000D-02	0.37291058	-67.336853	-47.925049	0.83687518
0.20999999D-02	0.30809526	-95.641357	-66.523651	0.69141650
0.27999999D-02	0.25433367	-118.76579	-79.942184	0.57076829
0.34999999D-02	0.22156389	-139.38919	-90.859680	0.49722730
0.41999999D-02	0.19931357	-161.39902	-103.16364	0.44729376
0.48999998D-02	0.17420662	-184.81674	-116.87544	0.39094948
0.55999998D-02	0.14526304	-206.76035	-129.11313	0.32598513
0.62999998D-02	0.12044459	-225.16721	-137.81412	0.27029828
0.69999998D-02	0.10447769	-241.86075	-144.80174	0.23446263
0.76999997D-02	0.92784818D-01	-260.04395	-153.27921	0.20822501
0.83999997D-02	0.79963504D-01	-279.00610	-162.53535	0.17945179
0.90999997D-02	0.67148309D-01	-295.66040	-169.48390	0.15069230
0.97999997D-02	0.58390654D-01	-309.73364	-173.85109	0.13103862
0.10500000D-01	0.53300152D-01	-325.09766	-179.50919	0.11961467
0.11200000D-01	0.47838059D-01	-343.04126	-187.74704	0.10735679
0.11900000D-01	0.40812233D-01	-360.36084	-195.36049	0.91589637D-01
0.12600000D-01	0.34672418D-01	-374.34473	-199.63864	0.77810640D-01
0.13300000D-01	0.31090515D-01	-387.34424	-202.93216	0.69772437D-01
0.14000000D-01	0.28363294D-01	-402.85815	-208.74031	0.63652086D-01
0.14699999D-01	0.24817223D-01	-419.19458	-215.37076	0.55694095D-01
0.15399999D-01	0.21277762D-01	-432.89648	-219.36664	0.47750941D-01
0.16099999D-01	0.19103545D-01	-444.93237	-221.69676	0.42871624D-01
0.16799999D-01	0.17686133D-01	-459.30444	-226.36281	0.39690709D-01
0.17499999D-01	0.15795463D-01	-475.34912	-232.70158	0.35447724D-01
0.18199999D-01	0.13682991D-01	-489.44092	-237.08757	0.30706974D-01
0.18899999D-01	0.12278938D-01	-501.76978	-239.71042	0.27556039D-01
0.19599999D-01	0.11344497D-01	-516.45386	-244.68874	0.25459662D-01
0.20299999D-01	0.99926160D-02	-533.23535	-251.76436	0.22425141D-01
0.20999999D-01	0.83141345D-02	-547.37207	-256.19507	0.18659541D-01

IDENTIFICATION PW-12

AREA UNDER PULSE = 0.72243856

RADIAN FREQUENCY	TRANSFORM MAGNITUDE	PHASE ANGLE (DEG)	PHASE ANGLE LESS DEAD TIME (DEG)	NORMALIZED MAGNITUDE
0.0	0.72243856	0.0	0.0	1.0000000
0.107000000D-02	0.70668252	-30.572586	-23.277130	0.97819047
0.214000000D-02	0.66109504	-60.837875	-46.246948	0.91508824
0.321000000D-02	0.59055034	-90.423096	-68.536697	0.81744023
0.428000000D-02	0.50265579	-118.80009	-89.618225	0.69577652
0.535000000D-02	0.40712758	-145.14111	-108.66377	0.56354630
0.642000000D-02	0.31519481	-168.11610	-124.34328	0.43629289
0.749000000D-02	0.23902336	-185.89561	-134.82732	0.33085632
0.856000000D-02	0.18958263	-197.65166	-139.28792	0.26242041
0.963000000D-02	0.16907675	-207.08212	-141.42293	0.23403617
0.107000000D-01	0.16519449	-220.14908	-147.19441	0.22866233
0.117700000D-01	0.16229058	-238.21991	-157.96973	0.22464275
0.128400000D-01	0.15228733	-259.33643	-171.79097	0.21079624
0.139100000D-01	0.13428994	-281.17310	-186.33202	0.18588424
0.149800000D-01	0.11153235	-301.52466	-199.38815	0.15438316
0.160500000D-01	0.892844920D-01	-318.17432	-208.74239	0.12358766
0.171200000D-01	0.730667010D-01	-329.94214	-213.21474	0.10113898
0.181900000D-01	0.654862440D-01	-339.57813	-215.55522	0.906461080D-01
0.192600000D-01	0.634891400D-01	-352.41870	-221.10025	0.878817150D-01
0.203300000D-01	0.616201570D-01	-370.20142	-231.58751	0.852946670D-01
0.214000000D-01	0.566120540D-01	-391.21826	-245.30890	0.783624480D-01
0.224700000D-01	0.480302800D-01	-412.92358	-259.71875	0.664835500D-01
0.235400000D-01	0.373742260D-01	-432.22583	-271.72559	0.517334320D-01
0.246100000D-01	0.274692020D-01	-444.63184	-276.83618	0.380228900D-01
0.256800000D-01	0.219712060D-01	-447.04321	-271.95215	0.304125600D-01
0.267500000D-01	0.222072920D-01	-449.46143	-267.07471	0.307393510D-01
0.278200000D-01	0.245496160D-01	-462.38843	-272.70630	0.339815970D-01
0.288900000D-01	0.255478650D-01	-483.01318	-286.03564	0.353633740D-01
0.299600000D-01	0.240959660D-01	-506.80615	-302.53296	0.333536550D-01
0.310300000D-01	0.204843160D-01	-530.47876	-318.91016	0.283544050D-01
0.321000000D-01	0.157636320D-01	-550.48193	-331.61792	0.218200310D-01

IDENTIFICATION PW-16

AREA UNDER PULSE = 0.57359156

RADIAN FREQUENCY	TRANSFORM MAGNITUDE	PHASE ANGLE (DEG)	PHASE ANGLE LESS DEAD TIME (DEG)	NORMALIZED MAGNITUDE
0.0	0.57359156	0.0	0.0	1.0000000
0.73999981D-03	0.56073912	-28.539093	-19.041763	0.97759304
0.14799996D-02	0.52544321	-56.281754	-37.287064	0.91605813
0.22199994D-02	0.47623473	-82.569305	-54.077286	0.83026802
0.29599993D-02	0.42338620	-107.10542	-69.116043	0.73813185
0.36999991D-02	0.37425673	-130.16856	-82.681839	0.65247950
0.44399989D-02	0.33030390	-152.45126	-95.467194	0.57585209
0.51799987D-02	0.28859428	-174.40454	-107.92314	0.50313551
0.59199985D-02	0.24660986	-195.66849	-119.68974	0.42993984
0.66599983D-02	0.20582097	-215.12776	-129.65167	0.35882846
0.73999981D-02	0.17131005	-231.70102	-136.72757	0.29866208
0.81399980D-02	0.14758257	-245.82005	-141.34926	0.25729558
0.88799978D-02	0.13361226	-259.87134	-145.90327	0.23293973
0.96199976D-02	0.12357111	-275.69800	-152.23265	0.21543398
0.10359970-01	0.11280234	-292.86377	-159.90102	0.19665969
0.11099997D-01	0.10086763	-309.87939	-167.41925	0.17585271
0.11839997D-01	0.89854625D-01	-325.94385	-173.98657	0.15665263
0.12579997D-01	0.81092378D-01	-341.73340	-180.27873	0.14137652
0.13319997D-01	0.73582854D-01	-358.44043	-187.48833	0.12828441
0.14059996D-01	0.65511612D-01	-376.13086	-195.68153	0.11421300
0.14799996D-01	0.56396348D-01	-393.54834	-203.60146	0.98321441D-01
0.15539996D-01	0.47429832D-01	-409.16650	-209.72229	0.82689208D-01
0.16279996D-01	0.40169418D-01	-422.61890	-213.67743	0.70031397D-01
0.17019996D-01	0.34949019D-01	-435.31934	-216.88045	0.60930148D-01
0.17759996D-01	0.30789349D-01	-448.69946	-220.76334	0.53678177D-01
0.18499995D-01	0.26842821D-01	-462.44263	-225.00903	0.46797796D-01
0.19239995D-01	0.23190056D-01	-475.47266	-228.54187	0.40429562D-01
0.19979995D-01	0.20200583D-01	-487.91309	-231.48482	0.35217714D-01
0.20719995D-01	0.17663051D-01	-501.04175	-235.11620	0.30793778D-01
0.21459995D-01	0.14987468D-01	-514.85767	-239.43489	0.26129164D-01
0.22199994D-01	0.12087557D-01	-526.77930	-241.85910	0.21073458D-01

IDENTIFICATION PW-20

AREA UNDER PULSE = 0.38949017

RADIAN FREQUENCY	TRANSFORM MAGNITUDE	PHASE ANGLE (DEG)	PHASE ANGLE LESS DEAD TIME (DEG)	NORMALIZED MAGNITUDE
0.0	0.38949017	0.0	0.0	1.0000000
0.47999993D-03	0.37342407	-31.421021	-24.463028	0.95875094
0.95999986D-03	0.33041413	-61.064911	-47.148926	0.84832469
0.14399998D-02	0.27469618	-86.957108	-66.083115	0.70527114
0.19199997D-02	0.22489212	-107.60271	-79.770721	0.57740128
0.23999996D-02	0.19383407	-124.41919	-89.629211	0.49766102
0.28799996D-02	0.17773682	-141.93654	-100.18855	0.45633197
0.33599995D-02	0.16278332	-162.29124	-113.58527	0.41793949
0.38399994D-02	0.14139635	-183.57768	-127.91371	0.36302931
0.43199994D-02	0.11640635	-202.53548	-139.91353	0.29886851
0.47999993D-02	0.95703655D-01	-217.16280	-147.58284	0.24571520
0.52799992D-02	0.83607920D-01	-229.64052	-153.10257	0.21465990
0.57599992D-02	0.76158081D-01	-244.10786	-160.61192	0.19553274
0.62399991D-02	0.67688699D-01	-260.59375	-170.14001	0.17378795
0.67199990D-02	0.57599745D-01	-275.89771	-178.48584	0.14788498
0.71999989D-02	0.49229500D-01	-287.84839	-183.47858	0.12639472
0.76799989D-02	0.44689797D-01	-298.74536	-187.41757	0.11473922
0.81599988D-02	0.41945006D-01	-312.32080	-194.03503	0.10769208
0.86399987D-02	0.38300287D-01	-328.14746	-202.90361	0.98334414D-01
0.91199987D-02	0.33676037D-01	-343.45947	-211.25758	0.86461840D-01
0.95999986D-02	0.29600223D-01	-357.17310	-218.01324	0.75997355D-01
0.10079999D-01	0.26573764D-01	-371.32690	-225.20906	0.68227046D-01
0.10559998D-01	0.23432011D-01	-387.58057	-234.50467	0.60160724D-01
0.11039998D-01	0.19314980D-01	-404.00562	-243.97180	0.49590416D-01
0.11519998D-01	0.14963161D-01	-416.17114	-249.17920	0.38417301D-01
0.11999998D-01	0.12021233D-01	-421.60669	-247.65694	0.30864021D-01
0.12479998D-01	0.10882352D-01	-426.25000	-245.34221	0.27939992D-01
0.12959998D-01	0.10150098D-01	-435.04541	-247.17961	0.26059960D-01
0.13439998D-01	0.91256525D-02	-444.02612	-249.20242	0.23429738D-01
0.13919998D-01	0.84706581D-02	-450.09082	-248.30904	0.21748066D-01
0.14399998D-01	0.85932861D-02	-458.10327	-249.36356	0.22062909D-01

APPENDIX E

TIME DOMAIN COMPARISON OF SAMPLE DATA AND MODEL PREDICTIONS

IDENTIFICATION PW-10

DATA POINT INDEX	t, sec. TIME	C'_A, g. moles/liter DATA IMPULSE RESP.	C'_A, g. moles/liter CALCULATED IMPULSE RESP.
0	0.0	0.0	0.0
1	12.000000	0.23480708D-04	0.27629016D-04
2	24.000000	0.25857051D-04	0.55456932D-04
3	36.000000	0.39106511D-04	0.83667472D-04
4	60.000000	0.75699936D-04	0.14181081D-03
5	84.000000	0.13858185D-03	0.20272314D-03
6	108.00000	0.21443538D-03	0.26612059D-03
7	144.00000	0.34176395D-03	0.36272338D-03
8	180.00000	0.45231497D-03	0.45372841D-03
9	216.00000	0.54279249D-03	0.52927429D-03
10	240.00000	0.58218697D-03	0.56682366D-03
11	264.00000	0.60700485D-03	0.59237329D-03
12	288.00000	0.62397984D-03	0.60569837D-03
13	312.00000	0.63099386D-03	0.60773253D-03
14	336.00000	0.63099386D-03	0.60037702D-03
15	360.00000	0.62197750D-03	0.58615561D-03
16	384.00000	0.60800067D-03	0.56778692D-03
17	408.00000	0.58317650D-03	0.54775889D-03
18	456.00000	0.54475432D-03	0.50960157D-03
19	516.00000	0.48913155D-03	0.47021460D-03
20	576.00000	0.42818114D-03	0.43124456D-03
21	696.00000	0.32266602D-03	0.33131513D-03
22	816.00000	0.23948451D-03	0.25737219D-03
23	936.00000	0.17983114D-03	0.20224766D-03
24	1056.0000	0.13347944D-03	0.14728620D-03
25	1176.0000	0.10706957D-03	0.11928809D-03
26	1296.0000	0.87559660D-04	0.86415628D-04
27	1536.0000	0.63718864D-04	0.53063805D-04
28	1776.0000	0.44993896D-04	0.31882716D-04
29	2016.0000	0.28328330D-04	0.16956861D-04
30	2256.0000	0.0	0.82655835D-05

IDENTIFICATION PW-12

DATA POINT INDEX	t, sec. TIME	C'_A, g. moles/liter DATA IMPULSE RESP.	C'_A, g. moles/liter CALCULATED IMPULSE RESP.
0	0.0	0.0	0.0
1	24.000000	0.11165703D-03	0.54217816D-04
2	48.000000	0.14485657D-03	0.15352687D-03
3	72.000000	0.25467901D-03	0.32544448D-03
4	96.000000	0.52710134D-03	0.56935232D-03
5	120.00000	0.89520961D-03	0.85696195D-03
6	144.00000	0.12119131D-02	0.11431788D-02
7	168.00000	0.14408522D-02	0.13825132D-02
8	192.00000	0.15820577D-02	0.15442147D-02
9	204.00000	0.16186053D-02	0.15925549D-02
10	216.00000	0.16400185D-02	0.16203377D-02
11	228.00000	0.16461485D-02	0.16298979D-02
12	240.00000	0.16400185D-02	0.16243677D-02
13	252.00000	0.16277726D-02	0.16072816D-02
14	264.00000	0.15972618D-02	0.15821801D-02
15	288.00000	0.15035740D-02	0.15200988D-02
16	312.00000	0.14319359D-02	0.14554268D-02
17	360.00000	0.12468514D-02	0.13281131D-02
18	420.00000	0.10430261D-02	0.11160988D-02
19	480.00000	0.89520961D-03	0.87299874D-03
20	540.00000	0.79514598D-03	0.70448519D-03
21	600.00000	0.67962054D-03	0.56937764D-03
22	720.00000	0.45031914D-03	0.32613356D-03
23	840.00000	0.22158604D-03	0.19370834D-03
24	912.00000	0.0	0.13378138D-03

IDENTIFICATION PW-16

DATA POINT INDEX	t, sec. TIME	C'_A, g. moles/liter DATA IMPULSE RESP.	C'_A, g. moles/liter CALCULATED IMPULSE RESP.
0	0.0	0.0	0.0
1	30.000000	0.78519792D-04	0.13308110D-03
2	54.000000	0.17630379D-03	0.24465511D-03
3	78.000000	0.31839381D-03	0.36326388D-03
4	102.00000	0.51263883D-03	0.48860031D-03
5	126.00000	0.63742418D-03	0.61753138D-03
6	174.00000	0.86218258D-03	0.86199141D-03
7	210.00000	0.10058568D-02	0.10045379D-02
8	234.00000	0.10931580D-02	0.10682267D-02
9	258.00000	0.11185671D-02	0.11030702D-02
10	282.00000	0.11058371D-02	0.11093300D-02
11	306.00000	0.10805295D-02	0.10902789D-02
12	330.00000	0.10305392D-02	0.10515048D-02
13	354.00000	0.98626548D-03	0.99982822D-03
14	414.00000	0.85053989D-03	0.85608392D-03
15	474.00000	0.71435049D-03	0.73556277D-03
16	594.00000	0.51903585D-03	0.52443139D-03
17	714.00000	0.36027771D-03	0.32106376D-03
18	834.00000	0.22580006D-03	0.22306915D-03
19	954.00000	0.11513090D-03	0.12807767D-03
20	1074.0000	0.63413157D-04	0.85655529D-04
21	1194.0000	0.43001826D-04	0.54044678D-04
22	1314.0000	0.32262746D-04	0.27699389D-04
23	1554.0000	0.31147050D-04	0.65013789D-05
24	1794.0000	0.0	0.21886374D-05

IDENTIFICATION PW-20

DATA POINT INDEX	t, sec. TIME	C'_A, g. moles/liter DATA IMPULSE RESP.	C'_A, g. moles/liter CALCULATED IMPULSE RESP.
0	0.0	0.0	0.0
1	24.000000	0.17544735D-04	0.26411947D-04
2	48.000000	0.19970859D-04	0.53134291D-04
3	84.000000	0.34015437D-04	0.94353714D-04
4	132.00000	0.80964004D-04	0.15202945D-03
5	192.00000	0.17317661D-03	0.22704852D-03
6	252.00000	0.25934470D-03	0.29924397D-03
7	312.00000	0.33898349D-03	0.35927363D-03
8	348.00000	0.36929338D-03	0.38583512D-03
9	384.00000	0.38716709D-03	0.40390602D-03
10	420.00000	0.39253570D-03	0.41329067D-03
11	456.00000	0.39790734D-03	0.41464077D-03
12	492.00000	0.39253570D-03	0.40931683D-03
13	528.00000	0.38716709D-03	0.39913145D-03
14	564.00000	0.38001337D-03	0.38603023D-03
15	624.00000	0.35858434D-03	0.36231497D-03
16	684.00000	0.32653171D-03	0.34044943D-03
17	804.00000	0.26461505D-03	0.30297083D-03
18	924.00000	0.21923269D-03	0.25939571D-03
19	1044.0000	0.18666768D-03	0.21172759D-03
20	1224.0000	0.12745311D-03	0.16421739D-03
21	1404.0000	0.90959205D-04	0.12360458D-03
22	1584.0000	0.75410135D-04	0.89564889D-04
23	1824.0000	0.56996374D-04	0.62258528D-04
24	2064.0000	0.47286230D-04	0.39742005D-04
25	2304.0000	0.41556879D-04	0.25382226D-04
26	3012.0000	0.0	0.64389341D-05

IDENTIFICATION PM-10 Figure 10 Data

DATA POINT INDEX	t, sec. TIME	C'_B, g. moles/liter DATA IMPULSE RESP.	C'_B, g. moles/liter CALCULATED IMPULSE RESP.
0	0.0	0.0	0.0
1	5.0000000	0.72180000D-03	0.61672041D-01
2	10.000000	0.97369000D-02	0.94029727D-01
3	15.000000	0.21894600D-01	0.88046694D-01
4	20.000000	0.30736900D-01	0.58973779D-01
5	26.000000	0.31759200D-01	0.28389419D-01
6	30.000000	0.32936900D-01	0.22109246D-01
7	37.000000	0.33202800D-01	0.29472969D-01
8	42.000000	0.31736900D-01	0.31816075D-01
9	50.000000	0.28872000D-01	0.18130929D-01
10	65.000000	0.25263000D-01	0.14222191D-01
11	80.000000	0.22036900D-01	0.75935708D-02
12	95.000000	0.17036900D-01	0.98452527D-02
13	115.00000	0.16120200D-01	0.25373688D-02
14	125.00000	0.13836900D-01	0.75595299D-02
15	155.00000	0.10105200D-01	0.59618115D-02
16	185.00000	0.73383000D-02	0.46292207D-02
17	215.00000	0.52932000D-02	0.34289972D-02
18	245.00000	0.37293000D-02	0.23346336D-02
19	275.00000	0.29369000D-02	0.13612448D-02
20	335.00000	0.18045000D-02	-0.11130580D-03
21	395.00000	0.12030000D-02	-0.82663592D-03
22	525.00000	0.72180000D-03	0.66011383D-03
23	695.00000	0.12030000D-03	0.60834492D-03
24	821.00000	0.0	-0.44476284D-03

IDENTIFICATION PM-10 Figure 11 Data

DATA POINT INDEX	t, sec. TIME	C'_B, g. moles/liter DATA IMPULSE RESP.	C'_B, g. moles/liter CALCULATED IMPULSE RESP.
0	0.0	0.0	0.0
1	5.0000000	0.72180000D-03	0.15454694D-01
2	10.000000	0.97369000D-02	0.25779128D-01
3	15.000000	0.21894600D-01	0.29072210D-01
4	20.000000	0.30736900D-01	0.27399190D-01
5	26.000000	0.31759200D-01	0.24272968D-01
6	30.000000	0.32936900D-01	0.23569698D-01
7	37.000000	0.33202800D-01	0.24487648D-01
8	42.000000	0.31736900D-01	0.24605384D-01
9	50.000000	0.28872000D-01	0.22102264D-01
10	65.000000	0.25263000D-01	0.19838942D-01
11	80.000000	0.22036900D-01	0.17262107D-01
12	95.000000	0.17036900D-01	0.15951011D-01
13	115.00000	0.16120200D-01	0.13076337D-01
14	125.00000	0.13836900D-01	0.12943230D-01
15	155.00000	0.10105200D-01	0.10575883D-01
16	185.00000	0.73383000D-02	0.85862633D-02
17	215.00000	0.52932000D-02	0.70103969D-02
18	245.00000	0.37293000D-02	0.59158083D-02
19	275.00000	0.29369000D-02	0.45506080D-02
20	335.00000	0.18045000D-02	0.17954721D-02
21	395.00000	0.12030000D-02	0.26430196D-03
22	525.00000	0.72180000D-03	-0.22635709D-03
23	695.00000	0.12030000D-03	0.51699652D-03
24	821.00000	0.0	0.17560726D-04